Comparison of tropospheric NO$_2$ columns from MAX-DOAS retrievals and regional air quality model simulations

Anne-Marlene Blechschmidt[1], Joaquim Arteta[2], Adriana Coman[3], Lyana Curier[4,*], Henk Eskes[5], Gilles Foret[3], Clio Gielen[6], Francois Hendrick[6], Virginie Marécal[2], Frédérik Meleux[7], Jonathan Parmentier[2], Enno Peters[1], Gaia Pinardi[6], Ankie J. M. Piters[5], Matthieu Plu[2], Andreas Richter[1], Mikhail Sofiev[8], Álvaro M. Valdebenito[9], Michel Van Roozendael[6], Julius Vira[8], Tim Vlemmix[10], and John P. Burrows[1]

[1]Institute of Environmental Physics, University of Bremen, IUP-UB, Bremen, Germany
[2]Centre National de Recherches Météorologiques, Météo-France-CNRS, UMR 3589, Toulouse, France
[3]Laboratoire Interuniversitaire des Systèmes Atmosphériques, CNRS/INSU UMR7583, Université Paris-Est Créteil et Université Paris Diderot, Institut Pierre Simon Laplace, Créteil, France
[4]TNO, Climate Air and Sustainability Unit, Utrecht, the Netherlands
[5]Royal Netherlands Meteorological Institute, KNMI, De Bilt, the Netherlands
[6]Royal Belgian Institute for Space Aeronomy, BIRA-IASB, Brussels, Belgium
[7]Institut National de l'Environnement et des RISques industriels, INERIS, Verneuil en Halatte, France
[8]Finnish Meteorological Institute, FMI, Helsinki, Finland
[9]Norwegian Meteorological Institute, MetNo, Oslo, Norway
[10]TU-Delft, Delft, the Netherlands
[*]now at: Faculty of Humanities and Sciences, Department of Biobased Materials, Maastricht University, Geleen, the Netherlands

Correspondence to: A.-M. Blechschmidt (anne.blechschmidt@iup.physik.uni-bremen.de)

Abstract. Tropospheric NO$_2$ is hazardous to human health and can lead to tropospheric ozone formation, eutrophication of ecosystems and acid rain production. It is therefore important to establish accurate data based on models and observations to understand and monitor tropospheric NO$_2$ concentrations on a regional and global scale.

In the present study, MAX-DOAS tropospheric NO$_2$ column retrievals from four European measurement stations are compared to regional model ensemble simulations. The latter are based on regional air quality models which contribute to the European regional ensemble forecasts and reanalyses of the operational Copernicus Atmosphere Monitoring Service (CAMS). Compared to other observational data usually applied for regional model validation, MAX-DOAS data is closer to the regional model data in terms of horizontal and vertical resolution and measurements are available during daylight.

In general, there is a good agreement between simulated and retrieved NO$_2$ column values for individual MAX-DOAS measurements with correlations between 45 and 75 % for tropospheric NO$_2$ VCDs, indicating that the model ensemble represents the emission and tropospheric chemistry of NOx (NO+NO$_2$) well. Pollution transport towards the stations is on average well represented by the models. However, large differences are found for individual pollution plumes. Seasonal cycles are overestimated, weekly cycles are reproduced well and diurnal cycles poorly represented by the model ensemble. In particular, simulated morning rush hour peaks are not confirmed by MAX-DOAS retrievals. Our results demonstrate that a large number of validation points are available from MAX-DOAS measurements, which should therefore be used more extensively in future regional air quality modelling studies.

Atmospheric
Chemistry
and Physics
Discussions

1 Introduction

Nitrogen dioxide (NO_2) is a key species for atmospheric chemistry. Photolysis of NO_2 leads to formation of tropospheric ozone. The latter is a major greenhouse gas and the main precursor of OH, which itself determines the oxidising capacity of the atmosphere. Oxidation to HNO_3 via reaction with OH (daytime) or ozone (nighttime) is the major sink of NO_2 in the tro-
5 posphere (Jacob, 1999) and results in acid rain and eutrophication of ecosystems, which are both harmful for the environment. Moreover, NO_2 can cause irritation of respiratory organs (http://www3.epa.gov/).

Within the troposphere, conversion of NO to NO_2 only takes about a minute during daytime. The sum of NO and NO_2 is called NOx, which is mainly emitted in the form of NO to the atmosphere. Main sources of NOx are fossil fuel combustion and biomass burning. Some NOx is also produced from lightning and microbial activity in soils.

10 The lifetime of NO_2 is only a few hours in the boundary layer but a few days in the upper troposphere, where less OH radicals are present (Ehhalt et al., 1992). Several studies (e.g. Stohl et al., 2003; Zien et al., 2014) have shown that in the free troposphere, NO_2 can be transported over larger distances and is hence not only important for regional but also for global air quality. Peroxyacyl nitrate (PAN) produced by photochemical oxidation of carbonyl compounds is not much affected by wet scavenging and can act as a reservoir of NO_2, especially during long-range transport. If the air masses descend away from their
15 source regions, PAN will decompose to NOx under the influence of, on average, higher temperatures at lower altitudes (Jacob, 1999).

Given the influence of NOx on air quality and climate through effects on radiation, it is of high environmental and scientific interest to accurately observe and simulate spatial distribution and time evolution of NO_2 concentrations in the troposphere. Simulating NO_2 is a challenge for numerical models as it is chemically very active and depends on many factors including for
20 example cloud cover which affects photolysis of this trace gas. Moreover, correct representation of NOx emissions adds a large uncertainty to the model output.

MAX-DOAS (Multi Axis Differential Optical Absorption Spectroscopy; e.g. Hoenninger et al., 2004; Wittrock et al., 2004) measurements have been used to investigate air pollution in many studies, including the FORMAT campaign in Northern Italy (Heckel et al., 2005; Wagner et al., 2011), the CINDI campaign in the Netherlands (Piters et al., 2012), campaigns in Canada
25 (Halla et al., 2011; Mendolia et al., 2013), China (e.g. Irie et al., 2011; Hendrick et al., 2014; Ma et al., 2013; Wang et al., 2014), during ship-borne measurements (Leser et al., 2003; Takashima et al., 2012; Peters et al., 2012).

MAX-DOAS observations of atmospheric composition are performed by taking measurements of the scattered sunlight at different elevation and sometimes also azimuthal angles. Depending on the viewing angle and solar position, the light path through the atmosphere is different, with the observation in the zenith direction usually providing the shortest light path
30 through the lower troposphere. Therefore, using zenith measurements as intensity of incident radiation and observations in other angles as intensity of transmitted radiation, the total amount of molecules of a certain species along the light path difference (zenith subtracted from non-zenith measurement), so called differential slant column densities, can be determined using Lambert Beer's law. These can be inverted to tropospheric columns and lower altitude tropospheric profiles by radiative transfer modelling and optimal estimation techniques.

A large number of studies applied MAX-DOAS data for satellite validation (e.g. Celarier et al., 2008; Valks et al., 2011; Irie et al., 2008; Irie et al., 2012; Ma et al., 2013; Lin et al., 2014; Kanaya et al., 2014; Pinardi et al., 2014) but up to now, comparisons to regional air quality model simulations of tropospheric NO_2 have, to our knowledge, only been carried out by Vlemmix et al. (2015) and Shaiganfar et al. (2015). Several studies compared regional air quality model simulations to satellite

5 data (e.g. Huijnen et al., 2010), although satellite data are usually only available at much coarser time steps compared to regional model data. In this respect, the advantage of MAX-DOAS retrievals compared to satellite retrievals is the high resolution in time. Moreover, several studies compared in-situ NO_2 data (e.g. Vautard et al., 2009; Colette et al., 2011; Mues et al., 2014) to regional model results, although in-situ data usually refer to a specific location (point measurements), whereas regional model results are available for a specific horizontal grid resolution and area depending on the model set up. According to Richter et

10 al. (2013) the horizontal averaging volume of MAX-DOAS data depends on aerosol loading, wavelength and viewing direction and ranges from a few kilometres in the polluted boundary layer up to 80 km from the top of a mountain under clean air conditions. As MAX-DOAS data represents a larger volume of air, it is much better suited for regional model validation than in-situ data. Another advantage of MAX-DOAS measurements is their ability to observe several pollution related species at the same time (e.g. NO_2, HCHO, CHOCHO, SO_2, aerosols, potentially also O_3) and to provide NO_2 data which is virtually

15 free of interferences from other species or nitrogen compounds such as NOy (NOx and other oxidised nitrogen species).

The purpose of the present study is to investigate the usefulness of applying MAX-DOAS measurements for validation of regional air quality models. Parts of this approach are already applied within scientific reports of the operational Copernicus Atmosphere Monitoring Service (CAMS, http://atmosphere.copernicus.eu/), see e.g. Blechschmidt et al. (2015) and Antonakaki et al. (2016), and in parts to model results provided on 8 output levels only, which introduces uncertainty to comparison

20 results. CAMS is the operational follow-up of the former GEMS (Global and regional Earth-system Monitoring using Satellite and in-situ data) (Hollingsworth et al., 2008) and three succeeding MACC (Monitoring Atmospheric Composition and Climate, http://www.gmes-atmosphere.eu/) projects. The global component of CAMS extends weather services of the ECMWF (European Centre for Medium-Range Weather Forecasts) with simulations of atmospheric trace gases and aerosols, while operational air quality forecasts and analyses for Europe are provided at much higher resolution through the regional component.

25 Hourly NO_2 vertical column densities (VCDs) from 6 different regional model runs based on 5 models which are used within CAMS will be compared to MAX-DOAS measurements from three urban and one rural European station: Bremen (operated by IUP-Bremen), De Bilt (operated by KNMI), Uccle and OHP (Observatoire de Haute-Provence) (the latter two operated by BIRA-IASB).

This study focusses on evaluating the usefulness of validating regional air quality models with MAX-DOAS observations in

30 terms of validation points arising from the comparisons. The reasons for differences between model results and observations found by the comparisons are discussed here only in a general sense and need to be further investigated e.g. by carrying out additional dedicated model runs in future modelling studies.

The manuscript starts with an overview of regional model and MAX-DOAS data (Section 2) followed by a description of the intercomparison method (Section 3). Intercomparison results are described and discussed in Section 4. Finally, a summary

35 and conclusions are given in Section 5.

Atmospheric
Chemistry
and Physics
Discussions

2 Data basis

2.1 Regional air quality model simulations

CHIMERE (Menut et al., 2013), LOTOS-EUROS (LOng Term Ozone Simulation - EURopean Operational Smog) (Schaap et al., 2008), EMEP MSC-W (European Monitoring and Evaluation Programme Meteorological Synthesizing Centre - West) (Simpson et al., 2012), MOCAGE (Model Of atmospheric Chemistry At larGE scale) (Josse et al., 2004; Guth et al., 2016) and SILAM (System for Integrated modeLling of Atmospheric coMposition) (Sofiev et al., 2006; Sofiev et al., 2015) contributed to the European regional ensemble forecasts (Marécal et al., 2015) and reanalyses of the former MACC projects and are currently used within CAMS. These models have been used in many studies for investigating atmospheric composition on a regional scale (e.g. Drobinski et al., 2007; Huijnen et al., 2010; Lacressonnière et al., 2014; Petetin et al., 2015; Solazzo et al., 2012; Watson et al., 2016; Zyryanov et al., 2012).

All of these models use ECMWF-IFS and MACC reanalysis (Innes et al., 2013) data as meteorological and chemical input data and boundary conditions, respectively. Anthropogenic emissions are taken from the MACC emissions database (Kuenen et al., 2011), GFAS (Kaiser et al., 2012) is used to account for fire emissions. The input to these models is thus consistent and hence, differences in model results are due to differences in the modelling code, model set up or due to different scalings of emissions e.g. to account for seasonal, diurnal and weekly cycles as well as emission heights. The model runs investigated in the present study were performed by different European institutions and are based on different horizontal and vertical grid spacings and chemistry schemes (see Table 1 for further details). Apart from SILAM, the models were run without chemical data assimilation. The SILAM simulations included assimilation of surface observations of NO_2 as described in Vira and Sofiev (2015).

Two different sets of EMEP model runs are investigated in this study. The first one uses the same setup as the other regional models described above and is termed EMEP-MACCEVA in the following. EVA (validated assessments for air quality in Europe) was a subproject of MACC dedicated to the development and implementation of operational yearly production of European air quality assessment reports (https://www.gmes-atmosphere.eu). The second set of simulations (called EMEP in the following) uses the same set-up as in the EMEP status reports (see http://www.emep.int) for each year based on the EMEP subdomain, ECMWF-IFS as meteorological driver, EMEP emissions, Fire INventory from NCAR version 1.0 (FINNv1; Wiedinmyer et al., 2011), initial conditions described by Schulz et al. (2013) for the years 2010-2011 and Fagerli et al. (2014) for 2012 and climatological boundary conditions described by Simpson et al. (2012).

According to Mues et al. (2014), chemistry transport models in general account for seasonal, daily and diurnal emission changes by applying average time profiles given for different energy sectors and regions to totals of annual emissions across the model domain. Temporal emission patterns used by the regional air quality models listed above are country and SNAP (Selected Nomenclature for Sources of Air Pollution) sector dependent and are based on Denier van der Gon et al. (2011). A list of the SNAP sectors is given by Bieser et al. (2011). Moreover, different vertical emission profiles are applied for each regional model. These are described in more detail by Bieser et al. (2011) for EMEP and CHIMERE, Simpson et al. (2003) for

SILAM and Thunis et al. (2010) for LOTOS-EUROS. For MOCAGE, emissions are injected into the five lowest model levels using a hyperbolic decay.

More details on specific model setups and scores with respect to surface observations, can be found in Marécal et al. (2015) and in the model specification/validation dossiers which are available online at:

5   http://www.gmes-atmosphere.eu/about/documentation/regional/.

2.2 MAX-DOAS retrievals

This study makes use of MAX-DOAS measurements from four different European stations: Bremen (Germany), De Bilt (the Netherlands), Uccle (Belgium), and OHP (France). Characteristics of the data available from the stations, such as exact location and time period of retrievals investigated here, are briefly summarized in Table 2 and will be described in the following.

10   De Bilt (52.10° N, 5.18° E) is the home town of KNMI, and located just outside the city of Utrecht. The De Bilt experimental research site is surrounded by local and regional roads, with a lot of traffic which can affect regional air quality significantly. According to Vlemmix et al. (2015), it can also be affected by pollution sources which are located more far away in the Rotterdam region to the south-west, Amsterdam to the north-west and the German Ruhr region to the south-west of De Bilt. The MAX-DOAS instrument operated at De Bilt is a commercial system obtained from Hoffmann Messtechnik. It has an Ocean

15   Optics spectrograph, diffraction grating and a CCD detector. It operates at a wavelength range of 400-600 nm. Differential slant columns are retrieved by the DOAS method, wavelength calibration and slit-function width are determined using a high-resolution solar spectrum. The choice of fitting parameters complies with the standards agreed by the MAX-DOAS community, following from homogenization efforts within e.g. CINDI, GEOMON, NORS and QA4ECV as much as possible. Air mass factor (AMF) calculations are performed with the DAK (Doubling Adding KNMI; De Haan et al., 1987; Stammes , 2001)

20   radiative transfer model. For De Bilt, averaging kernels refer to the altitude-dependent (or box-)differential AMFs divided by the total differential AMF. The differential AMF is derived at a specific altitude by simulating the radiance with and without an added partial column of NO_2 at this altitude with the DAK model.

The IUP-Bremen MAX-DOAS instrument consists of an outdoor telescope unit collecting light in different directions, and an indoor grating spectrometer (Shamrock 163 equipped with an Andor LOT257U CCD with 2048x512 pixels) covering a

25   wavelength interval from 430–516 nm at a resolution of approximately 0.7 nm. Both components are connected via an optical fiber bundle which simplifies handling and overcomes polarization effects. The telescope unit is installed at an altitude of approximately 20 m above ground level at the roof of the Institute of Environmental Physics building (53.11° N, 8.86° E) at the University of Bremen which is located to the north-east of the city centre. The azimuthal pointing direction is north-west, which means that some of the measured pollution peaks are due to the exhaust of an industrial area, predominantly a steel plant, as

30   well as a near-by highway. However, averages over longer time periods should be dominated by pollution from the city centre. NO_2 slant column densities are obtained from a DOAS analysis using a fitting window from 450-497 nm and elevation angles ranging from 0° to 15° in 1° steps as well as at 30° elevation angle and zenith direction (used as a reference). Cross sections of O_3, NO_2, O_4, H_2O and a pseudo cross-section accounting for the Ring effect are applied. Resulting slant columns of NO_2 and O_4 are then input to the BRemian Advanced MAX-DOAS retrieval algorithm (BREAM), which is a two-step approach. First,

Atmospheric
Chemistry
and Physics
Discussions

an aerosol extinction profile is retrieved by comparing the measured O_4 slant columns to O_4 slant columns simulated using the radiative transfer model SCIATRAN (Rozanov et al. , 2005). In the second step, the derived aerosol extinction, measured NO_2 slant columns and an apriori NO_2 profile are used to retrieve the NO_2 profile of interest. This is an inverse problem solved by means of the optimal estimation method (Rodgers , 2000). Detailed information about the profile retrieval can be found in

5   Wittrock et al. (2006) and Peters et al. (2012).

BIRA-IASB operates a MAX-DOAS instrument at OHP (Observatoire de Haute-Provence; 43.92° N, 5.7° E) since 2005. OHP is a background remote site in the south of France, temporarily affected by transport of pollution from regional sources (e.g. from the petrochemical plants of Etang de Berre close to Marseille in the south-west) and the Po valley (Italy) to the north-east of the station. The MAX-DOAS instrument, which points towards the SSW direction, consists of a grating spectrometer

10   covering a wavelength range of 330-390 nm and collecting photons at 4°, 5°, 6°, 8°, 10°, 15°, 30° and 90° (zenith) viewing elevation angles. NO_2 differential slant column densities (DSCDs) are obtained by applying the DOAS technique to a 364-384 nm wavelength interval, taking into account spectral signatures of O_3, O_4, the Ring effect and NO_2 at 298 K. For the retrieval of aerosol extinction profiles (see below), O_4 is fitted to a wavelength interval of 338-370 nm including O_3, HCHO, BrO, the Ring effect and O_4 absorption cross-sections.

15   At Uccle, which is located south-west of the Brussels city centre, a mini-MAX-DOAS from Hoffmann Messtechnik GmbH covering the 290-435 nm wavelength range is operated by BIRA-IASB since 2011. The instrument is pointing northwards towards the city centre and scans the following elevation angles: 3°, 4°, 5°, 6°, 7°, 9°, 11°, 13°, 16°, 31° and zenith. NO_2 and O_4 DSCDs are retrieved in 407-432 and 350-384 nm wavelength intervals, respectively, including the same spectral signatures as for OHP. It should be noted that a sequential zenith reference spectrum has been implemented in order to minimise the

20   impact of changes in shift and resolution due to temperature instabilities. The DOAS fit for NO_2 has also been improved by introducing pseudo-absorber cross-sections derived from principal component analysis of residuals on days affected by large thermal instabilities. This approach allows for a better correction of fast-changing slit-function variations, resulting in more stable residuals and therefore more realistic random uncertainty estimates.

For NO_2 vertical profile retrievals at both stations, the bePRO radiative transfer code (Clémer et al., 2010) is used, which is

25   an inversion algorithm based on the optimal estimation method (Rodgers , 2000) and consists of a two-step approach. Firstly, the model uses observed MAX-DOAS O_4 DSCDs to derive vertical profiles of aerosol extinction at different wavelengths. In the second step, NO_2 vertical profiles are derived from NO_2 DSCDs and the previously retrieved information on aerosol profiles. A more detailed description of the model and trace gas profile retrievals can be found in Hendrick et al. (2014).

NO_2 profiles are retrieved at 420 nm for Uccle and 372 nm for OHP. For NO_2 vertical profile retrievals, exponentially

30   decreasing a-priori profiles have been constructed, based on a first estimation of NO_2 vertical column densities derived from the so-called geometrical approximation (Hoenninger et al., 2004; Brinksma et al., 2008) and using scaling heights of 0.5 and 1 km for OHP and Uccle, respectively. A-priori and measurement-uncertainty covariance matrices are constructed as by Clémer et al. (2010) with adopted correlation lengths of 0.05, and covariance scaling values of 0.5 and 0.35 for Uccle and OHP, respectively. Pressure and temperature profiles were taken from the US Standard Atmosphere and the retrieval grid consists

35   of ten layers of 200 m thickness between the station altitude and 2 km altitude, two layers of 500 m thickness between 2 and

3 km and 1 layer between 3 and 4 km altitude. For this study, only retrievals with a residual of the optimal estimation method retrieval fit to the DSCDs smaller than 50 % and degrees of freedom for signal larger than 1 are used.

Previous studies (e.g. Hendrick et al., 2014; Wang et al., 2014; Franco et al., 2015) have shown that the typical error on MAX-DOAS retrieved VCDs is around 20 %, including uncertainties related to the optimal estimation method, trace gas cross sections and aerosol retrievals, and can be higher for sites with low trace gas concentrations like OHP or due to instrumental conditions.

For Uccle, information on cloud conditions (i.e. clear-sky, thin clouds, thick clouds, broken clouds) was retrieved according to the method by Gielen et al. (2014) which is based on analysis of the MAX-DOAS retrievals. The presence of clouds may alter MAX-DOAS retrievals in several ways: (1) If clouds are present at both zenith and horizon viewing directions, NO_2 within and above the clouds is shielded from the MAX-DOAS view whereas the sensitivity is slightly increased below the cloud, (2) if a cloud is present at the zenith/non-zenith viewing direction only, the sensitivity is reduced/enhanced at the height of the cloud and slightly enhanced/reduced below the cloud compared to the cloud free case. The impact of clouds on MAX-DOAS retrievals is described in detail by Vlemmix et al. (2015). In addition to the direct effect of clouds on the measurements, clouds also affect photolysis rates and hence NOx chemistry and NO to NO_2 partitioning, which may have an impact on tropospheric NO_2 columns and profiles retrieved under cloudy weather conditions.

2.3 Wind measurements

In order to investigate the ability of the models to reproduce transport of NO_2 towards the stations, the data described above is complemented by meteorological in-situ station data of wind speed and wind direction. Wind data for Bremen was provided by the German Weather Service/ Deutscher Wetterdienst through their website at http://www.dwd.de. The weather station in Bremen is located at the main airport, approximately 9 km southwards of the MAX-DOAS station. This may result in some differences to the actual wind direction and wind speed at time and location of the MAX-DOAS retrievals. Wind data for OHP was taken from the weather station at the observatory and downloaded from the corresponding website at http://pc-meteo.obs-hp.fr/intervalle.php. Wind speed and direction measurements at Uccle are performed using a commercial rugged wind sensor from Young (model 05103) and were provided by BIRA-IASB through their webpage at http://uvindex.aeronomie.be.

3 Intercomparison method

The sensitivity of MAX-DOAS retrievals is largest in the boundary layer, which needs to be taken into account when comparing MAX-DOAS retrievals to model simulated values. This is achieved here, by applying column averaging kernels (AVKs) to the model data prior to comparison. The AVKs are part of the MAX-DOAS profiling output and represent the sensitivity of the retrieved column to the amount of NO_2 at different altitudes. Note that no profile data is available for De Bilt and AVKs were derived based on (box-)differential AMFs at that station (see Section 2.2).

Atmospheric
Chemistry
and Physics
Discussions

In this study, model VCDs are derived by two different methods in order to test the influence of AVKs on the data analysis. Model VCDs are calculated by simply summing up NO_2 partial columns (VCD_i) over all N model levels in the vertical (method 1):

$$VCD_{method\,1}^{model} = \sum_{i=1}^{N\,model} VCD_i^{model} \tag{1}$$

5   In addition, model VCDs are calculated by applying column AVKs of the retrievals to model NO_2 partial columns before summing up NO_2 partial columns in the vertical (method 2). The following data processing steps were carried out prior to the application of column AVKs:

(1) Conversion of provided model NO_2 partial columns [molec cm^{-2}] to concentrations [molec cm^{-3}] using model layer thicknesses.

10   (2) Deriving model concentrations on measurement altitudes assuming that model concentrations are constant within a specific model layer. If a measurement layer overlaps with more than one model layer, the result is a weighted mean over the model layer concentrations. If the highest measurement altitude is above the model top, the concentration at the model top level is used. It is assumed here that the latter has no significant impact on the data analysis, as NO_2 concentrations are in general small towards higher elevation levels compared to lower levels.

15   (3) Conversion of derived NO_2 concentrations on measurement altitudes to partial columns [molec cm^{-2}] using observation layer thicknesses.

Model VCDs for method 2 were then calculated using the following equation:

$$VCD_{method\,2}^{model} = \sum_{i=1}^{N\,obs} AVK_i * VCD_i^{model} \tag{2}$$

where Nobs is the number of measurement altitudes.

20   Note that method 1 and method 2 use the model output at original vertical resolution. VCDs are calculated separately for each model and constitute the basis for calculating ensemble mean values which are described at the end of this Section.

Only those model values closest to the measurement time are used below. As the model output is given in hourly time steps, the maximum possible time difference between measurements and simulations is 30 minutes.

Following studies by e.g., Marécal et al. (2015), Langner et al. (2012), Solazzo et al. (2012), Vautard et al. (2009), the present

25   manuscript focuses on results of the model ensemble, i.e. the median of individual model results of a given quantity, for the sake of simplicity and in order to reduce individual model outliers. As an even number of 6 different model runs (based on 5 different models) constitute the model ensemble in the present study, the median is calculated by ordering the 6 different model values (e.g. for seasonal cycles, these values refer to the average of individual model runs for each month) in terms of magnitude and taking the average of the two middle numbers. An exception is OHP as MOCAGE data is not available for this

30   station so that the median refers to the middle number here. Standard deviations are calculated based on results from individual

ensemble members (i.e. results prior to calculation of model ensemble mean values) and are used as an indicator of how much individual ensemble members differ from each other. In addition, results from separate models are briefly discussed where needed to understand characteristics of the model ensemble output. However, it is beyond the scope of this study to describe the performance of each individual model in detail. The reader is referred to the Appendix for comparison Figures of individual

5   model simulations and MAX-DOAS data. As the typical error on MAX-DOAS retrieved VCDs is around 20 %, but can be higher for sites with low trace gas concentrations like OHP or due to instrumental conditions (see Section 2.2), a conservative overall uncertainty of MAX-DOAS retrievals of 30 % is assumed for all stations within this manuscript and given along with the data plots, where appropriate.

4   Intercomparison results

10   Figures 1 and 2 show time series of tropospheric NO_2 VCDs derived by method 1 and 2 as well as surface partial columns (i.e. the partial column of the lowest measurement layer) from MAX-DOAS and model ensemble data. As vertical profiles are not available from the MAX-DOAS output for De Bilt, comparisons of profiles and surface partial columns are not given for this station in the present manuscript. The magnitude of VCDs from the measurements for Bremen and OHP is reproduced by the model ensemble (using either method 1 or method 2). Model ensemble values are generally lower than the observed ones for

15   Uccle and especially for De Bilt. However, at all of the four stations, measurements and simulations show large deviations for some of the time steps investigated. Some of the larger NO_2 values inside individual pollution plumes are underestimated by the model ensemble. The model ensemble may fail to reproduce these peaks due to errors in transport of NO_2 towards the stations or incomplete representation of atmospheric chemistry. An example of the latter would be overestimation of conversion to HNO_3, which may result in lower tropospheric NO_2 VCDs compared to MAX-DOAS if the transport is not happening quickly

20   enough. Moreover, differences between simulations and retrievals may also arise from uncertainties of anthropogenic NOx emissions and horizontal resolution of model results (e.g. pollution sources may not be sufficiently resolved by the model simulations). Colette et al. (2014) compared regional model simulations with differing horizontal resolution and found that an increase in resolution leads to a better agreement with NO_2 in-situ data. However, as described in Section 1, MAX-DOAS observations are closer to regional model output in horizontal resolution than in-situ data.

25   As expected, the magnitude of NO_2 VCDs is lowest at the rural station OHP, which is sometimes affected by local pollution plumes that show up in the time series. Further investigation shows, that most of these peaks are associated with north-easterly wind directions and hence pollution sources to the north-east of the station such as the Po valley (Italy). Applying column AVKs to model data for calculating VCDs (method 2) compared to method 1 does not have a big impact on validation results. Statistical values (root mean squared error, bias, correlation) which will be described below are quite similar for AVK weighted

30   model ensemble values and those from method 1. The evolution of time series of tropospheric NO_2 VCDs is largely determined by the evolution of surface partial columns. Looking at the time series, surface partial columns already account for about 25 % of the magnitude of tropospheric NO_2 VCDs. The same conclusions as for tropospheric NO_2 VCDs described in this paragraph arise for surface partial columns when comparing model ensemble to MAX-DOAS data.

Although there are large differences for individual data points, Figure 3 shows that frequency distributions of tropospheric NO_2 VCDs are similar for simulations and observations. However, for OHP the number of data values with tropospheric NO_2 VCDs lower than 1 x 10^{15} molec cm^{-2} is significantly larger for model simulated values (about 1400 model values compared to about 200 observed data counts).

5   As the sensitivity of MAX-DOAS retrievals is largest in the boundary layer, we initially expected the application of column AVKs from the measurements to model simulations to be of crucial importance for validation results. Therefore, the results described above at first instance are surprising but can be explained when comparing model ensemble to MAX-DOAS vertical profiles of partial columns averaged over the whole time period of measurements shown in Figure 4 (a). Averages of vertical profiles over three months are given in Figures 4 (b) to (e), in order to investigate consistency between profiles throughout

10 different seasons. A-priori profiles assumed within the DOAS retrievals and AVKs are included in the plots for completeness. Differences between retrievals and simulations are largest for larger NO_2 partial columns, which means for the lower altitude layers and during the colder winter and autumn seasons. Many of the model simulated values do not fall into the uncertainty range of MAX-DOAS retrievals assumed here. Although model ensemble profiles show some differences to the retrievals regarding the exact shape and magnitude of the profiles, they also show the largest partial columns close to the surface for all

15 of the three stations investigated. This result also shows up throughout different seasons. This means that the main source of the scatter between measurements and simulations is not due to the vertical representativeness of the observations and as such, application of column AVKs has a minor effect on the data analysis presented in this manuscript.

    Individual model runs consistently show low partial columns at higher altitudes and disagree much more for values close to the surface, i.e. closer to NOx emission sources, which is expressed by generally larger standard deviations at lower altitudes.

20 The seasonal variation of vertical profiles is reproduced by the model ensemble.

    Figure 4 (f) shows comparisons for Uccle only, but for MAX-DOAS measurements carried out under different cloud conditions (i.e., from left to right: clear-sky, thin clouds, thick clouds) as derived from the MAX-DOAS observations (Gielen et al., 2014; see Section 2.2). On average, observed NO_2 partial columns are higher in the lowest observation layers during cloudy conditions compared to clear-sky conditions. Further investigation shows, that this feature is consistent throughout different

25 seasons, except for MAM months for which only 3 % of the observations were made under clear-sky conditions, whereas during other seasons, about 10 to 15 % of the observations were made under clear-sky conditions. In theory, below a cloud less light and hence less OH is present in the lowest observations layers, which acts as a sink for NO_2 during daytime. Moreover, less NO_2 is photolysed below a cloud. The model ensemble reproduces the overall change of NO_2 partial columns from clear-sky to thin cloud conditions for the lowest observation layer. The strong simulated decrease in values from thin cloud to thick

30 cloud conditions is not confirmed by the retrievals. To find out the reason for this would require further investigation, but could point to errors in simulating photochemistry under cloudy conditions.

    In the following, only results from method 2 will be discussed. As shown above, these do not differ substantially from method 1 comparisons, which is true for all results presented below.

    Scatter density plots of tropospheric NO_2 VCDs from MAX-DOAS against model values corresponding to the time series

35 displayed by Figures 1 and 2 (b) are shown in Figure 5 (a). Scatter density plots of surface partial columns corresponding to

time series in Figures 1 and 2 (c) are shown in Figure 5 (b). Statistical values (root mean squared error, bias, correlation) and least squares regression lines are given along with the plots in Figure 5 to draw further conclusions on the ability of the model ensemble to reproduce MAX-DOAS retrievals. Moderate correlations of 45 to 75 % are found for tropospheric NO_2 VCDs for all stations, the highest correlation is found for Uccle. Correlations are lower for surface partial columns which are on the

5   order of 40 % for Bremen and OHP, but much higher for Uccle ($\sim$60 %). The model ensemble has a negative bias of about 0.3 and 2 x 10^{15} molec cm^{-2} for OHP and Uccle, respectively, and a positive bias of about 1 x 10^{15} molec cm^{-2} for De Bilt and Bremen for tropospheric columns. For surface partial columns, biases are negligibly small for OHP and Bremen, while the ensemble is negatively biased by about 1 x 10^{15} molec cm^{-2} at Uccle. The spread between models and observations is large for some individual data points. Regression lines show that the model ensemble tends to overestimate low and underestimate

10 high tropospheric NO_2 VCD and surface partial column retrievals. The underestimation of larger tropospheric NO_2 VCDs is most pronounced for De Bilt, followed by Uccle.

Figure 6 shows comparisons for wind directional distributions of average tropospheric NO_2 VCDs and surface partial columns for the different stations. Changes of NO_2 mean values from one wind direction bin to another are reproduced well by the model ensemble, with an overall slightly better agreement with retrievals for tropospheric NO_2 VCDs compared to surface

15 partial columns. Both, MAX-DOAS and model ensemble show the highest NO_2 mean values for wind directions mainly where influence from pollution sources is expected (i.e. Ruhr area to the south-east of De Bilt, the Bremen city centre to the south-west of the Bremen MAX-DOAS, Brussels city centre to the north-east of Uccle, the Po valley to the north-east of OHP, see Section 2.2). As for the time series comparisons described above, differences between observations and model results could be related to model uncertainties in simulating transport of pollution towards the measurement stations and chemistry. Uncertain-

20 ties in anthropogenic emissions and background NO_2 VCDs may add up to differences between models and MAX-DOAS for wind directional distributions.

Comparisons for seasonal cycles (i.e. monthly averages) of tropospheric NO_2 VCDs are given in Figure 7. The number of MAX-DOAS measurements available for each month is given at the top y-axis of each plot as an indicator of statistical significance. The number of data values is also shown for diurnal and weekly cycle Figures which will be discussed below.

25 There is a good agreement between MAX-DOAS and the model ensemble for Uccle regarding the magnitude of NO_2 VCDs and seasonality, with simulated values within the estimated uncertainty interval of the retrievals. The same is true for De Bilt, apart from the strong overestimation of MAX-DOAS retrieved values for January, March and April. The latter may be explained by the low number of observations available during these compared to other months. The model ensemble overestimates seasonal cycles for Bremen and OHP. More explicitly, there is an overestimation of wintertime values while summertime values are

30 better reproduced by the model ensemble. This may indicate that the model ensemble overestimates production of OH via photolysis of O_3 when less light is available, as OH acts as a sink for NO_2. The latter may also result from errors in simulating clouds and related photochemistry during the colder season. It may also point to an overestimation of anthropogenic emissions or inappropriate scalings of these. The former would be in agreement with Petetin et al. (2015), who found that anthropogenic NOx emissions from the TNO emission inventory (on which MACC emissions are based on) are overestimated, but those

35 results apply to the Paris region only. Huijnen et al. (2010) compared an ensemble of regional and global models to satellite

data over Europe and found an overestimation of seasonal cycles by the simulations, which is in agreement with results for Bremen and OHP shown in the present manuscript. However, according to Huijnen et al. (2010) model values were closer to satellite retrievals during winter, whereas for summer a strong underestimation was found, while comparisons to Dutch surface observations showed that this could be partly attributed to a high bias of satellite retrievals in summer at least over the

5   Netherlands. In the present study, wintertime standard deviations are quite large for OHP indicating that some of the models perform better compared to others (see Figure A11 for corresponding individual model results). Results for SILAM agree with Vira and Sofiev (2015) who found that this model tends to overestimate NO_2 at rural sites based on in-situ data.

Figures 8 and 9 (a) show comparisons of diurnal cycles for the whole time series. Overall, the model ensemble fails to reproduce diurnal cycles for all stations. Although most of the model values fall within the estimated uncertainty interval of

10 MAX-DOAS retrievals, the shape of diurnal cycles differs from each other. While the model ensemble tends to simulate a decrease in tropospheric NO_2 VCDs from the morning to the afternoon for all stations, MAX-DOAS retrieved values generally increase towards the afternoon. Moreover, the ensemble shows a strong peak during the morning rush hour around 8 am for Bremen, which is not confirmed by MAX-DOAS retrievals. In contrast to this, measurements show a maximum around 2 pm in the afternoon which coincides with a very weak local maximum simulated by the model ensemble. Looking at diurnal cycles

15 for different seasons shown in Figures 8 and 9 (b) to (e) reveals that these are in general much better reproduced for spring and summer compared to autumn and winter for all stations. This is in agreement with results for seasonal cycles described in the previous paragraph. Weak morning rush hour peaks are also simulated for the rural station OHP, which is not in agreement with the measurements. Inspection of corresponding individual model results (see Figures A12 and A13) shows that the morning rush hour peaks for Bremen and OHP occur for all models with the exception of SILAM for OHP, which however strongly

20 overestimates values (by a factor of 1.5 to 2 for diurnal cycle values averaged over the whole time series) for this station. Individual model runs show the same shape of the diurnal cycle for Bremen, while the shape of diurnal cycles differs for OHP. Moreover, large differences regarding the magnitude of simulated values occur for both stations. As described in Section 2.1, all models use the same emission scenario as a basis, except EMEP. The differences in diurnal cycles between model simulations and retrievals as well as between individual model runs could mean that the different scalings of NOx emissions applied by

25 each model to account for diurnal variations are not appropriate, maybe in combination with uncertainties in vertical scalings. This should be investigated in future modelling studies. For example, according to Mailler et al. (2013) improving efficient emission heights is a key factor for improving background atmospheric composition simulated by chemistry transport models. However, the disagreement between simulated and measured values as well as the disagreement between individual model runs may also point to problems regarding photochemistry and treatment of boundary layer mixing. Differences in transport

30 of pollution towards the stations during the morning and evening may add up to model uncertainties, especially for the rural station OHP where different shapes of diurnal cycles for individual model runs may also result from pollution transported from urban surrounding areas towards the station.

Weekly cycle comparisons are presented in Figures 10 and 11 for the whole time series and for different seasons. In contrast to diurnal cycles, weekly cycles and their seasonal variation measured by MAX-DOAS are much better simulated, with a small

35 underestimation by the models compared to the retrievals. Both, MAX-DOAS and the model ensemble, show a decrease in

tropospheric NO_2 VCDs towards the weekend when there is less traffic especially for the urban stations De Bilt, Bremen and Uccle. However, the observed decrease is stronger than the simulated one, a feature which is most pronounced for Bremen. Note that maxima of weekly cycles for specific days may just be coincidence due to data sampling times.

5 Summary and conclusions

5 In this study, comparisons between NO_2 columns simulated by a regional model ensemble and retrieved from MAX-DOAS measurements for four European MAX-DOAS stations have been presented.

This study focusses on evaluating the usefulness of validating regional air quality models with MAX-DOAS observations in terms of validation points arising from the comparisons. The reasons for differences between model results and observations found by the comparisons are discussed here only in a general sense and need to be further investigated by carrying out

10 additional dedicated model runs in future modelling studies. In general, differences between simulated and retrieved tropospheric NO_2 VCDs as well as surface partial columns found in this study could result from model uncertainties in chemistry and meteorology or a combination of both. Moreover, errors in the NOx emission inventories or uncertainties in tropospheric MAX-DOAS retrievals may also contribute to differences between simulated and retrieved values found in this study.

Our analysis shows that in general and on average the model ensemble does well represent emissions and tropospheric

15 chemistry of NOx. However, many validation points arise from the MAX-DOAS based comparisons which could improve model performance substantially. Moderate correlations around 60 % are found for tropospheric NO_2 VCDs at each station. Time series comparisons and corresponding scatterplots show that uncertainties in simulating pollution transport towards the stations is a likely reason for the underestimation of MAX-DOAS retrieved pollution peaks by the model ensemble. This may also lead to the weak simulated morning rush hour peak for the rural station OHP, which is not confirmed by the retrievals. In

20 fact, for OHP, a diurnal cycle representative of a remote background NO_2 station would be expected. However, comparisons of wind directional distributions of tropospheric NO_2 VCDs and surface partial columns show a good agreement between simulations and measurements. This indicates that transport of pollution towards the stations is, on average, well represented by the models.

Comparisons of vertical profiles show that the main source of the scatter between measurements and simulations is not the

25 correct representation of the vertical NO_2 distribution. Hence, there are no large differences between comparisons which do not make use of column AVKs for calculating model VCDs and those based on more accurate column AVK weighted values. The latter result was not expected as the sensitivity of the MAX-DOAS profile retrievals is much larger close to the surface than at altitudes larger than approximately 1 km.

Seasonal cycles are overestimated by the model ensemble. Simulation uncertainties in photochemistry are a conceivable

30 explanation for this. As MAX-DOAS measurements are carried out throughout the whole course of a day during daylight, it is possible to compare diurnal cycles derived from simulations and measurements. This reveals that models fail to reproduce the shape of diurnal cycles for all stations, which most likely points to uncertainties in diurnal scaling of emissions. Improving model results for diurnal cycles could potentially have a strong impact on all other comparisons shown in this manuscript and

Atmospheric
Chemistry
and Physics
Discussions

hence may further improve model performance. This is in agreement with Mues et al. (2014) who found an improvement of correlations between LOTOS-EUROS and in-situ data when applying a time profile to emissions. However, weekly cycles are well represented by the model ensemble, indicating that scalings of emissions on a daily basis are appropriate.

Our evaluation demonstrates that the large number of measurements available from the current MAX-DOAS network con-
5   stitutes a useful data source for validation of regional models. In contrast to other measurements usually applied for validation of regional models, MAX-DOAS data are available with comparatively high resolution in time. Furthermore, MAX-DOAS retrievals are representative of a larger volume of air and are therefore much better suited for regional model validation than in-situ data. Nevertheless, it would be desirable to complement and compare results of this study by other data sources where possible. Future investigations of regional model performance may also include application of stricter quality filters on the
10   MAX-DOAS data to reduce the impact of retrieval uncertainty. The impact of different model set-ups and different anthropogenic emission inventories as well as horizontal and vertical scalings of the latter on validation results should be tested in order to improve model performance. As the discussion here is based on results from five regional models used within CAMS for four European stations, similar comparisons to other regional models as well as for more MAX-DOAS stations should follow.

15   **6   Code availability**

Source code and test data sets for the Open Source EMEP/MSC-W model are available at https://github.com/metno/emep-ctm or by contacting EMEP/MSC-W (emep.mscw@met.no). The SILAM code is available on request from the authors (mikhail.sofiev@fmi.fi, julius.vira@fmi.fi). The MOCAGE results in the present paper are based on source code which is presently incorporated in the MOCAGE model. The MOCAGE source code is the property of Météo-France and CERFACS,
20   and it is based on libraries that belong to some other holders. The MOCAGE model is not open source and routines from MOCAGE cannot be freely distributed. CHIMERE is an open source code protected under the GNU General Public license. It can be found at http://www.lmd.polytechnique.fr/chimere/. LOTOS-EUROS is downloadable free of charge after signing a license agreement. All information concerning the LOTOS-EUROS code is available on the website (http://lotos-euros.nl), for further information the reader can contact Dr. A. Manders (astrid.manders@tno.nl).

Atmospheric
Chemistry
and Physics
Discussions

References

Antonakaki, T., Blechschmidt, A.-M., Clark, H., Gielen, C., Hendrick, F., Kapsomenakis, J., Mortier, A., Peters, E., Piters, A., Richter, A., van Roozendael, M., Schulz, M., Wagner, A., Zerefos, C., and Eskes, H. J.: Validation of CAMS regional services: concentrations above the surface, CAMS report, 30 June 2016, 2016.

5 Beirle, S., Platt, U., Wenig, M., and Wagner, T.: Weekly cycle of NO_2 by GOME measurements: a signature of anthropogenic sources, Atmos. Chem. Phys., 3, 2225-2232, doi:10.5194/acp-3-2225-2003, 2003.

Bergström, R., Denier van der Gon, H.A.C., Prevot, A.S.H., Yttri, K.E. and Simpson, D.: Modelling of organic aerosols over Europe (2002-2007) using a volatility basis set (VBS) framework with application of different assumptions regarding the formation of secondary organic aerosol, Atmos. Chem. Physics, 12, 5425–5485, 2012.

10 Bieser, J., Aulinger, A., Matthias, V., Quante, M., and Denier van Der Gon, H. A. C.: Vertical emission profiles for Europe based on plume rise calculations, Environmental Pollution 159 (10), 2935-2946, 2011.

Blechschmidt, A.-M., Coman, A., Curier, L., Eskes, H. J., Foret, G., Gielen, C., Hendrick, F., Marecal, V., Meleux, F., Parmentier, J., Peters, E., Pinardi, G., Piters, A., Plu, M., Richter, A., Sofiev, M., Valdebenito, Á. M., Van Roozendael, M., Vira, J., and Vlemmix, T.: MAX-DOAS tropospheric NO_2 column retrievals as a validation tool for regional air quality models of the upcoming Copernicus Atmosphere

15 Monitoring Service, CAMS report, 30 September 2015, 2015.

Brinksma, E.J., Pinardi, G. J., Braak, R., Volten, H., Richter, A., Dirksen, R. J., Vlemmix, T., Swart, D. P. J., Knap, W. H., Veefkind, J. P., Eskes, H. J., Allaart, M., Rothe, R., Piters, A. J. M., and Levelt, P.F.: The 2005 and 2006 DANDELIONS NO_2 and Aerosol Intercomparison Campaigns. J. Geophys. Res.,113, D16S46, doi:10.1029/2007JD008808, 2008.

Celarier, E. A., Brinksma, E. J., Gleason, J. F., Veefkind, J. P., Cede, A, Herman, J. R., Ionov, D., Goutail, F., Pommereau, J.-P., Lambert,

20 J.-C., van Roozendael, M., Pinardi, G., Wittrock, F., Schönhardt, A., Richter, A., Ibrahim, O. W. , Wagner, T., Bojkov, B., Mount, G., Spinei, E., Chen, C. M. Pongetti, T. J. , Sander, S. P., Bucsela, E. J., Wenig, M. O. , Swart, D. P. J., Volten, H., Kroon, M., and Levelt, P. F.: Validation of Ozone Monitoring Instrument nitrogen dioxide columns, J. Geophys. Res., 113, D15S15, doi:10.1029/2007JD008908, 2008.

Clémer, K., Van Roozendael, M., Fayt, C., Hendrick, F., Hermans, C., Pinardi, G., Spurr, R., Wang, P., and De Mazière, M.: Multiple

25 wavelength retrieval of tropospheric aerosol optical properties from MAXDOAS measurements in Beijing, Atmos. Meas. Tech., 3, 863-878, doi:10.5194/amt-3-863-2010, 2010.

Colette, A., Granier, C., Hodnebrog, Ø., Jakobs, H., Maurizi, A., Nyiri, A., Bessagnet, B., D'Angiola, A., D'Isidoro, M., Gauss, M., Meleux, F., Memmesheimer, M., Mieville, A., Rouïl, L., Russo, F., Solberg, S., Stordal, F., and Tampieri, F.: Air quality trends in Europe over the past decade: a first multimodel assessment, Atmos. Chem. Phys., 11, 11657–11678, doi:10.5194/acp-11-11657-2011, 2011.

30 Colette, A., Bessagnet, B., Meleux, F., Terrenoire, E., and Rouïl, L.: Frontiers in air quality modelling, Geosci. Model Dev., 7, 203-210, doi:10.5194/gmd-7-203-2014, 2014.

Curier, R. L., Timmermans, R., Calabretta-Jongen, S., Eskes, H., Segers, A., Swart, D., and Schaap, M: Improving ozone forecasts over Europe by synergistic use of the LOTOS-EUROS chemical transport model and in situ measurements. Atmos. Environ, 60, 217–226, 2012.

35 Curier, R. L., Kranenburg, R., Segers, A., Timmermans, R., and Schaap, M.: Synergistic use of OMI-NO_2 tropospheric columns and LOTOS-EUROS to evaluate the NOx emission trends across Europe, Remote Sens. Environ., 149, 58 69,doi:10.1016/j.rse.2014.03.032, 2014.

Atmospheric
Chemistry
and Physics
Discussions

Open Access

EGU

De Haan, J.F., Bosma, P.B., and Hovenier, J.W.: The adding method for multiple scattering calculations of polarized light, Astron. Astrophys., 183, 371-393, 1987.

Denier van der Gon, H. A. C., Hendriks, C., Kuenen, J., Segers, A. and Visschedijk, A.: Description of current temporal emission patterns and sensitivity of predicted AQ for temporal emission patterns, TNO report, EU FP7 MACC deliverable report D_D-EMIS_1.3, Utrecht,

5   the Netherlands, 2011.

Drobinski, P., Saïd, F., Ancellet, G., Arteta, J., Augustin, P., Bastin, S., Brut, A., Caccia, J., Campistron, B., Cautenet, S., Colette, A., Coll, I., Corsmeier, U., Cros, B., Dabas, A., Delbarre, H., Dufour, A., Durand, P., Gu enard, V., Hasel, M., Kalthoff, N., Kottmeier, C., Lasry, F., Lemonsu, A., Lohou, F., Masson, V., Menut, L., Moppert, C., Peuch, V., Puygrenier, V., Reitebuch, O., and Vautard, R.: Regional transport and dilution during high-pollution episodes in southern France: Summary of findings from the Field Experiment to Constraint Models of

10   Atmospheric Pollution and Emissions Transport (ESCOMPTE), J. Geophys. Res., 112, D13105, doi:10.1029/2006JD007494, 2007.

Ehhalt, D. H., Rohrer, F., and Wahner, A.: Sources and Distribution of NOx in the Upper Troposphere at Northern Mid-Latitudes, J. Geophys. Res., 97, 3725–3738, http://www.agu.org/journals/jd/v097/iD04/91JD03081/, 1992.

Fagerli, H., Solberg, S., Tsyro, S., Benedictow, A., Aas, W., Hjellbrekke, A.-G. and Posch, M.: Status of transboundary pollution in 2012, Transboundary particulate matter, photo-oxidants, acidifying and eutrophying components, EMEP Status Report 1/2014, The Norwegian

15   Meteorological Institute, Oslo, Norway, 2014.

Franco, B., Hendrick, F., Van Roozendael, M., Müller, J.-F., Stavrakou, T., Marais, E. A., Bovy, B., Bader, W., Fayt, C., Hermans, C., Lejeune, B., Pinardi, G., Servais, C., and Mahieu, E.: Retrievals of formaldehyde from ground-based FTIR and MAX-DOAS observations at the Jungfraujoch station and comparisons with GEOS-Chem and IMAGES model simulations, Atmos. Meas. Tech., 8, 1733-1756, doi:10.5194/amt-8-1733-2015, 2015.

20   Gielen, C., Van Roozendael, M., Hendrick, F., Pinardi, G., Vlemmix, T., De Bock, V., De Backer, H., Fayt, C., Hermans, C., Gillotay, D., and Wang, P.: A simple and versatile cloud-screening method for MAX-DOAS retrievals, Atmos. Meas. Tech., 7, 3509-3527, doi:10.5194/amt-7-3509-2014, 2014.

Guth, J., Josse, B., Marécal, V., Joly, M., and Hamer, P.: First implementation of secondary inorganic aerosols in the MOCAGE version R2.15.0 chemistry transport model, Geosci. Model Dev., 9, 137-160, doi:10.5194/gmd-9-137-2016, 2016.

25   Halla, J. D., Wagner, T., Beirle, S., Brook, J. R., Hayden, K. L., O'Brien, J. M., Ng, A., Majonis, D., Wenig, M. O., and McLaren, R.: Determination of tropospheric vertical columns of NO_2 and aerosol optical properties in a rural setting using MAX-DOAS, Atmos. Chem. Phys., 11, 12475-12498, doi:10.5194/acp-11-12475-2011, 2011.

Heckel, A., Richter, A., Tarsu, T., Wittrock, F., Hak, C., Pundt, I., Junkermann, W., and Burrows, J. P.: MAX-DOAS measurements of formaldehyde in the Po-Valley, Atmos. Chem. Phys., 5, 909–918, 2005.

30   Hendrick, F., Müller, J.-F., Clémer, K., Wang, P., De Mazière, M., Fayt, C., Gielen, C., Hermans, C., Ma, J. Z., Pinardi, G., Stavrakou, T., Vlemmix, T., and Van Roozendael, M.: Four years of ground-based MAX-DOAS observations of HONO and NO_2 in the Beijing area, Atmos. Chem. Phys., 14, 765–781, doi:10.5194/acp-14-765-2014, 2014.

Hönninger, G., von Friedeburg, C., and Platt, U.: Multi axis differential optical absorption spectroscopy (MAX-DOAS), Atmos. Chem. Phys., 4, 231-254, doi:10.5194/acp-4-231-2004, 2004.

35   Hollingsworth, A. R., Engelen, R. J., Textor, C., Benedetti, A., Boucher, O., Chevallier, F., Dethof, A., Elbern, H., Eskes, H., Flemming, J., Granier, C., Kaiser, J. W., Morcrette, J.-J., Rayner, P., Peuch, V.-H., Rouil, L., Schultz, M. G., Simmons, A. J., and Consortium, T. G.: Toward a monitoring and forecasting system for atmospheric composition: The GEMS project, B. Am. Meteorol. Soc., 89, 1147–1164, 2008.

Huijnen, V., Eskes, H. J., Poupkou, A., Elbern, H., Boersma, K. F., Foret, G., Sofiev, M., Valdebenito, A., Flemming, J., Stein, O., Gross, A., Robertson, L., D'Isidoro, M., Kioutsioukis, I., Friese, E., Amstrup, B., Bergstrom, R., Strunk, A., Vira, J., Zyryanov, D., Maurizi, A., Melas, D., Peuch, V.-H., and Zerefos, C.: Comparison of OMI NO$_2$ tropospheric columns with an ensemble of global and European regional air quality models, Atmos. Chem. Phys., 10, 3273-3296, doi:10.5194/acp-10-3273-2010, 2010.

5 Inness, A., Baier, F., Benedetti, A., Bouarar, I., Chabrillat, S., Clark, H., Clerbaux, C., Coheur, P., Engelen, R. J., Errera, Q., Flemming, J., George, M., Granier, C., Hadji-Lazaro, J., Huijnen, V., Hurtmans, D., Jones, L., Kaiser, J. W., Kapsomenakis, J., Lefever, K., Leitão, J., Razinger, M., Richter, A., Schultz, M. G., Simmons, A. J., Suttie, M., Stein, O., Thépaut, J.-N., Thouret, V., Vrekoussis, M., Zerefos, C., and the MACC team: The MACC reanalysis: an 8 yr data set of atmospheric composition, Atmos. Chem. Phys., 13, 4073-4109, doi:10.5194/acp-13-4073-2013, 2013.

10 Irie, H., Kanaya, Y., Akimoto, H., Tanimoto, H., Wang, Z., Gleason, J. F., and Bucsela, E. J.: Validation of OMI tropospheric NO$_2$ column data using MAX-DOAS measurements deep inside the North China Plain in June 2006: Mount Tai Experiment 2006, Atmos. Chem. Phys., 8, 6577-6586, doi:10.5194/acp-8-6577-2008, 2008.

Irie, H., Takashima, H., Kanaya, Y., Boersma, K. F., Gast, L., Wittrock, F., Brunner, D., Zhou, Y., and Van Roozendael, M.: Eight-component retrievals from ground-based MAX-DOAS observations, Atmos. Meas. Tech., 4, 1027–1044, doi:10.5194/amt-4-1027-2011, 2011.

15 Irie, H., Boersma, K. F., Kanaya, Y., Takashima, H., Pan, X., and Wang, Z. F.: Quantitative bias estimates for tropospheric NO$_2$ columns retrieved from SCIAMACHY, OMI, and GOME-2 using a common standard for East Asia, Atmos. Meas. Tech., 5, 2403-2411, doi:10.5194/amt-5-2403-2012, 2012.

Jacob, D. J.: Introduction of Atmospheric Chemistry, Princeton Univ. Press, Princeton, NJ, 234-243, 1999.

Josse, B., Simon, P., and Peuch, V.-H.: Radon global simulations with the multiscale chemistry and transport model MOCAGE, Tellus B, 56, 339–356. doi: 10.1111/j.1600-0889.2004.00112.x, 2004.

20

Kaiser, J. W., Heil, A., Andreae, M. O., Benedetti, A., Chubarova, N., Jones, L., Morcrette, J.-J., Razinger, M., Schultz, M. G., Suttie, M., and van der Werf, G. R.: Biomass burning emissions estimated with a global fire assimilation system based on observed fire radiative power, Biogeosciences, 9, 527–554, doi:10.5194/bg-9-527-2012, 2012.

Kanaya, Y., Irie, H., Takashima, H., Iwabuchi, H., Akimoto, H., Sudo, K., Gu, M., Chong, J., Kim, Y. J., Lee, H., Li, A., Si, F., Xu, J.,
25 Xie, P.-H., Liu, W.-Q., Dzhola, A., Postylyakov, O., Ivanov, V., Grechko, E., Terpugova, S., and Panchenko, M.: Long-term MAX-DOAS network observations of NO$_2$ in Russia and Asia (MADRAS) during the period 2007–2012: instrumentation, elucidation of climatology, and comparisons with OMI satellite observations and global model simulations, Atmos. Chem. Phys., 14, 7909-7927, doi:10.5194/acp-14-7909-2014, 2014.

Kramer, L. J., Leigh, R. J., Remedios, J. J. and Monks, P. S.: Comparison of OMI and ground-based in situ and MAX-DOAS measurements
30 of tropospheric nitrogen dioxide in an urban area, J. Geophys. Res., 113, D16S39, doi:10.1029/2007JD009168, 2008.

Kuenen, J. J. P., Denier van der Gon, H. A. C., Visschedijk, A., Van der Brugh, H., and Van Gijlswijk, R.: MACC European emission inventory for the years 2003–2007, TNO report TNO-060-UT-2011-00588, Utrecht, 2011.

Lacressonnière, G., Peuch, V.-H., Vautard, R., Arteta, J., Déqué, M., Josse, B., Marécal, V., and Saint-Martin, D.: European air quality in the 2030s and 2050s: Impacts of global and regional emission trends and of climate change, Atmos. Environ., 92, 348–358, 2014.

35 Langner, J., Engardt, M., Baklanov, A., Christensen, J. H., Gauss, M., Geels, C., Hedegaard, G. B., Nuterman, R., Simpson, D., Soares, J., Sofiev, M., Wind, P., and Zakey, A.: A multi-model study of impacts of climate change on surface ozone in Europe, Atmos. Chem. Phys., 12, 10423-10440, doi:10.5194/acp-12-10423-2012, 2012.

Atmospheric
Chemistry
and Physics
Discussions

Lefèvre, F., Brasseur, G., Folkins, I., Smith, A., and Simon, P.: Chemistry of the 1991–1992 stratospheric winter: three-dimensional model simulations, J. Geophys. Res.-Atmos., 99, 8183–8195, 1994.

Leser, H., Hönninger, G. and Platt, U.: MAX-DOAS measurements of BrO and NO_2 in the marine boundary layer, Geophys. Res. Lett., 30(10), 1537, doi:10.1029/2002GL015811, 2003.

5 Lin, J.-T., Martin, R. V., Boersma, K. F., Sneep, M., Stammes, P., Spurr, R., Wang, P., Van Roozendael, M., Clémer, K., and Irie, H.: Retrieving tropospheric nitrogen dioxide from the Ozone Monitoring Instrument: effects of aerosols, surface reflectance anisotropy, and vertical profile of nitrogen dioxide, Atmos. Chem. Phys., 14, 1441-1461, doi:10.5194/acp-14-1441-2014, 2014.

Ma, J. Z., Beirle, S., Jin, J. L., Shaiganfar, R., Yan, P., and Wagner, T.: Tropospheric NO_2 vertical column densities over Beijing: results of the first three years of ground-based MAX-DOAS measurements (2008–2011) and satellite validation, Atmos. Chem. Phys., 13, 1547-1567,
10 doi:10.5194/acp-13-1547-2013, 2013.

Mailler, S., Khvorostyanov, D., and Menut, L.: Impact of the vertical emission profiles on background gas-phase pollution simulated from the EMEP emissions over Europe, Atmos. Chem. Phys., 13, 5987-5998, doi:10.5194/acp-13-5987-2013, 2013.

Marécal, V., Peuch, V.-H., Andersson, C., Andersson, S., Arteta, J., Beekmann, M., Benedictow, A., Bergström, R., Bessagnet, B., Cansado, A., Chéroux, F., Colette, A., Coman, A., Curier, R. L., Denier van der Gon, H. A. C., Drouin, A., Elbern, H., Emili, E., Engelen, R.
15 J., Eskes, H. J., Foret, G., Friese, E., Gauss, M., Giannaros, C., Guth, J., Joly, M., Jaumouillé, E., Josse, B., Kadygrov, N., Kaiser, J. W., Krajsek, K., Kuenen, J., Kumar, U., Liora, N., Lopez, E., Malherbe, L., Martinez, I., Melas, D., Meleux, F., Menut, L., Moinat, P., Morales, T., Parmentier, J., Piacentini, A., Plu, M., Poupkou, A., Queguiner, S., Robertson, L., Rouïl, L., Schaap, M., Segers, A., Sofiev, M., Tarasson, L., Thomas, M., Timmermans, R., Valdebenito, Á., van Velthoven, P., van Versendaal, R., Vira, J., and Ung, A.: A regional air quality forecasting system over Europe: the MACC-II daily ensemble production, Geosci. Model Dev., 8, 2777-2813,
20 doi:10.5194/gmd-8-2777-2015, 2015.

Mendolia, D., D'Souza, R. J. C., Evans, G. J., and Brook, J.: Comparison of tropospheric NO_2 vertical columns in an urban environment using satellite, multi-axis differential optical absorption spectroscopy, and in situ measurements, Atmos. Meas. Tech., 6, 2907-2924, doi:10.5194/amt-6-2907-2013, 2013.

Menut, L., Bessagnet, B., Khvorostyanov, D., Beekmann, M., Blond, N., Colette, A., Coll, I., Curci, G., Foret, G., Hodzic, A., Mailler, S.,
25 Meleux, F., Monge, J. L., Pison, I., Siour, G., Turquety, S., Valari, M., Vautard, R., and Vivanco, M. G.: CHIMERE 2013: a model for regional atmospheric composition modelling, Geoscientific Model Development, 6, 981-1028, doi:10.5194/gmd-6-981-2013, 2013.

Mues, A., Kuenen, J., Hendriks, C., Manders, A., Segers, A., Scholz, Y., Hueglin, C., Builtjes, P., and Schaap, M.: Sensitivity of air pollution simulations with LOTOS-EUROS to the temporal distribution of anthropogenic emissions, Atmos. Chem. Phys., 14, 939-955, doi:10.5194/acp-14-939-2014, 2014.

30 Peters, E., Wittrock, F., Großmann, K., Frieß, U., Richter, A., and Burrows, J. P.: Formaldehyde and nitrogen dioxide over the remote western Pacific Ocean: SCIAMACHY and GOME-2 validation using ship-based MAX-DOAS observations, Atmos. Chem. Phys., 12, 11179-11197, doi:10.5194/acp-12-11179-2012, 2012.

Petetin, H., Beekmann, M., Colomb, A., Denier van der Gon, H. A. C., Dupont, J.-C., Honoré, C., Michoud, V., Morille, Y., Perrussel, O., Schwarzenboeck, A., Sciare, J., Wiedensohler, A., and Zhang, Q. J.: Evaluating BC and NOx emission inventories for the Paris region
35 from MEGAPOLI aircraft measurements, Atmos. Chem. Phys., 15, 9799-9818, doi:10.5194/acp-15-9799-2015, 2015.

Pinardi, G., Van Roozendael, M., Lambert, J.-C., Granville, J., Hendrick, F., Tack, F., Yu, H., Cede, A., Kanaya, Y., Irie, H., Goutail, F., Pommereau, J.-P., Pazmino, A., Wittrock, F., Richter, A., Wagner, T., Gu, M., Remmers, J., Friess, U., Vlemmix, T., Piters, A., Hao, N., Tiefengraber, M., Herman, J., Abuhassan, N., Bais, A., Kouremeti, N., Hovila, J., Holla, R., Chong, J., Postylyakov, O. and Ma, J.:

GOME-2 total and tropospheric NO$_2$ validation based on zenith-sky, direct-sun and Multi-Axis DOAS network observations, EUMETSAT conference, Geneva, Switzerland, 22-26 September 2014.

Piters, A. J. M., Boersma, K. F., Kroon, M., Hains, J. C., Van Roozendael, M., Wittrock, F., Abuhassan, N., Adams, C., Akrami, M., Allaart, M. A. F., Apituley, A., Beirle, S., Bergwerff, J. B., Berkhout, A. J. C., Brunner, D., Cede, A., Chong, J., Clémer, K., Fayt, C., Frieß, U., Gast, L. F. L., Gil-Ojeda, M., Goutail, F., Graves, R., Griesfeller, A., Großmann, K., Hemerijckx, G., Hendrick, F., Henzing, B., Herman, J., Hermans, C., Hoexum, M., van der Hoff, G. R., Irie, H., Johnston, P. V., Kanaya, Y., Kim, Y. J., Klein Baltink, H., Kreher, K., de Leeuw, G., Leigh, R., Merlaud, A., Moerman, M. M., Monks, P. S., Mount, G. H., Navarro-Comas, M., Oetjen, H., Pazmino, A., Perez-Camacho, M., Peters, E., du Piesanie, A., Pinardi, G., Puentedura, O., Richter, A., Roscoe, H. K., Schönhardt, A., Schwarzenbach, B., Shaiganfar, R., Sluis, W., Spinei, E., Stolk, A. P., Strong, K., Swart, D. P. J., Takashima, H., Vlemmix, T., Vrekoussis, M., Wagner, T., Whyte, C., Wilson, K. M., Yela, M., Yilmaz, S., Zieger, P., and Zhou, Y.: The Cabauw Intercomparison campaign for Nitrogen Dioxide measuring Instruments (CINDI): design, execution, and early results, Atmos. Meas. Tech., 5, 457-485, doi:10.5194/amt-5-457-2012, 2012.

Richter, A., Godin, S., Gomez, L., Hendrick, F., Hocke, K., Langerock, B., van Roozendael, M., Wagner, T.: Spatial Representativeness of NORS observations, NORS project deliverable, available online at: http://nors.aeronomie.be/projectdir/PDF/D4.4_NORS_SR.pdf, 2013.

Rodgers, C. D.: Inverse Methods for Atmospheric Sounding – Theory and Practice, Series on Atmospheric, Oceanic and Planetary Physics, World Scientific, Singapore, 2000.

Rozanov, A., Rozanov, V., Buchwitz, M., Kokhanovsky, A., and Burrows, J. P.: SCIATRAN 2.0 – a new radiative transfer model for geophysical applications in the 175–2400 nm spectral region, Adv. Space Res., 36, 1015–1019, 2005.

Schaap, M., Timmermans, R. M. A., Roemer, M., Boersen, G. A. C., Builtjes, P. J. H., Sauter, F. J., Velders, G. J. M., Beck, J .P: The LOTOS-EUROS Model: Description, validation and latest developments. Int. J. Environ. Pollut., 32, 270–290, 2008.

Schaap, M., Kranenburg, R., Curier, L., Jozwicka, M., Dammers, E., and Timmermans, R.: Assessing the Sensitivity of the OMI-NO$_2$ Product to Emission Changes across Europe, Remote Sensing, 5(9), 4187-4208, doi:10.3390/rs5094187, 2013.

Schmidt, H., Derognat, C., Vautard, R., and Beekmann, M.: A comparison of simulated and observed ozone mixing ratios for the summer of 1998 in western Europe, Atmos. Environ., 35, 6277–6297, 2001.

Schulz, M., Benedictow, A., Schneider, P., Bartnicki, J., Valdebenito, Á., Gauss, M. and Griesfeller, J.: Modelling and evaluation of trends in the EMEP framework, Transboundary acidification, eutrophication and ground level ozone in Europe in 2011, EMEP Status Report 1/2013, The Norwegian Meteorological Institute, Oslo, Norway, 2013.

Shaiganfar, R., Beirle, S., Petetin, H., Zhang, Q., Beekmann, M., and Wagner, T.: New concepts for the comparison of tropospheric NO$_2$ column densities derived from car-MAX-DOAS observations, OMI satellite observations and the regional model CHIMERE during two MEGAPOLI campaigns in Paris 2009/10, Atmos. Meas. Tech., 8, 2827-2852, doi:10.5194/amt-8-2827-2015, 2015.

Simpson, D., Benedictow, A., Berge, H., Bergström, R., Emberson, L. D., Fagerli, H., Flechard, C. R., Hayman, G. D., Gauss, M., Jonson, J. E., Jenkin, M. E., Nyíri, A., Richter, C., Semeena, V. S., Tsyro, S., Tuovinen, J.-P., Valdebenito, Á., and Wind, P.: The EMEP MSC-W chemical transport model – technical description, Atmos. Chem. Phys., 12, 7825-7865, doi:10.5194/acp-12-7825-2012, 2012.

Simpson, D., Fagerli, H., Jonson, J., Tsyro, S., Wind, P., and Tuovinen, J.-P.: The EMEP Unified Eulerian Model. Model Description, EMEP MSC-W Report 1/2003, The Norwegian Meteorological Institute, Oslo, Norway, 2003.

Sofiev, M.: A model for the evaluation of long-term airborne pollution transport at regional and continental scales, Atmos. Env., 34(15), 24812493, doi:10.1016/S1352-2310(99)00415-X, 2000.

Sofiev, M., Siljamo, P., Valkama, I., Ilvonen, M., and Kukkonen, J.:. A dispersion modelling system SILAM and its evaluation against ETEX data, Atmos. Environ. 40, 674–685, doi:10.1016/j.atmosenv.2005.09.069, 2006.

Atmospheric
Chemistry
and Physics
Discussions

Sofiev, M., Vira, J., Kouznetsov, R., Prank, M., Soares, J., and Genikhovich, E.: Construction of an Eulerian atmospheric dispersion model based on the advection algorithm of M . Galperin: dynamic cores, Geosci. Model Dev. Discuss., 8, 2905–2947, doi:10.5194/gmdd-8-2905-2015, 2015.

Solazzo, E., Bianconi, R., Vautard, R., Appel, K. W., Moran, M. D., Hogrefe, C., Bessagnet, B., Brandt, J., Christensen, J. H., Chemel, C., Coll, I., Denier van der Gon, H., Ferreira, J., Forkel, R., Francis, X. V., Grell, G., Grossi, P., Hansen, A. B., Jeričević, A., Kraljević, L., Miranda, A. I., Nopmongcol, U., Pirovano, G., Prank, :, Riccio, A., Sartelet, K. N., Schaap, M., Silver, J. D., Sokhi, R. S., Vira, J., Werhahn, J., Wolke , R., Yarwood, G., Zhang, J., Rao, S. T., and Galmarini, S.: Model Evaluation and Ensemble Modeling of Surface-Level Ozone in Europe and North America in the Context of the AQMEII, Atmos. Environ., 53, 60-74, 2012.

Solomon, S.: Stratospheric ozone depletion: a review of concepts and history, Rev. Geophys., 37, 275–316, 1999.

Stammes, P.: Spectral radiance modeling in the UV-visible range, in: IRS 2000: Current Problems in Atmospheric Radiation, edited by: Smith, W. and Timofeyev, Y. A. Deepak, Hampton, Va, 385–388, 2001.

Stockwell, W., Kirchner, F., Kuhn, M., and Seefeld, S.: A new mechanism for regional atmospheric chemistry modeling, J. Geophys. Res., 102, 25847–25879, 1997.

Stohl, A., Huntrieser, H., Richter, A., Beirle, S., Cooper, O. R., Eckhardt, S., Forster, C., James, P., Spichtinger, N., and Wenig, M.: Rapid intercontinental air pollution transport associated with a meteorological bomb, Atmos. Chem. Phys., 3, 969–985, http://www.atmos-chem-phys.net/3/969/2003/, 2003.

Takashima, H., Irie, H., Kanaya, Y., and Syamsudin, F.: NO_2 observations over the western Pacific and Indian Ocean by MAX-DOAS on Kaiyo, a Japanese research vessel, Atmos. Meas. Tech., 5, 2351-2360, doi:10.5194/amt-5-2351-2012, 2012.

Thunis, P., Cuvelier, C., Roberts, P., White, L., Stern, R., Kerschbaumer, A.,Bessagnet, B., Bergström, R., and Schaap, M.: EURODELTA: Evaluation of a Sectoral Approach to Integrated Assessment Modelling- Second Report. In: EUR -Scientific and Technical Research Series -24474 EN-2010, Publications Office of the European Union, Luxembourg, ISSN 1018-5593, 2010.

Valks, P., Pinardi, G., Richter, A., Lambert, J.-C., Hao, N., Loyola, D., Van Roozendael, M., and Emmadi, S.: Operational total and tropospheric NO_2 column retrieval for GOME-2, Atmos. Meas. Tech., 4, 1491-1514, doi:10.5194/amt-4-1491-2011, 2011.

Vautard, R., Schaap, M., Bergström, R., Bessagnet, B., Brandt, J., Builtjes, P. J. H., Christensen, J. H., Cuvelier, K., Foltescu, V., Graff, A., Kerschbaumer, A., Krol, M., Roberts, P., Rouil, L., Stern, R., Tarrasón, L., Thunis, P., Vignati, E., Wind, P.: Skill and uncertainty of a regional air quality model ensemble, Atmos. Env. 43, 4822-4832, doi:10.1016/j.atmosenv.2008.09.083, 2009.

Vira, J. and Sofiev, M.: Assimilation of surface NO_2 and O_3 observations into the SILAM chemistry transport model. Geosci. Model Dev. 8, 191–203, doi:10.5194/gmd-8-191-2015, 2015.

Vlemmix, T., Eskes, H. J., Piters, A. J. M., Schaap, M., Sauter, F. J., Kelder, H., and Levelt, P. F.: MAX-DOAS tropospheric nitrogen dioxide column measurements compared with the Lotos-Euros air quality model, Atmos. Chem. Phys., 15, 1313-1330, doi:10.5194/acp-15-1313-2015, 2015.

Wagner, T., Beirle, S., Brauers, T., Deutschmann, T., Frieß, U., Hak, C., Halla, J. D., Heue, K. P., Junkermann, W., Li, X., Platt, U., and Pundt-Gruber, I.: Inversion of tropospheric profiles of aerosol extinction and HCHO and NO_2 mixing ratios from MAX-DOAS observations in Milano during the summer of 2003 and comparison with independent data sets, Atmos. Meas. Tech., 4, 2685–2715, doi:10.5194/amt-4-2685-2011, 2011.

Wang, T., Hendrick, F., Wang, P., Tang, G., Clémer, K., Yu, H., Fayt, C., Hermans, C., Gielen, C., Pinardi, G., Theys, N., Brenot, H., and Van Roozendael, M.: Evaluation of tropospheric SO2 retrieved from MAX-DOAS measurements in Xianghe, China, Atmos. Chem. Phys. Discuss., 14, 6501-6536, doi:10.5194/acpd-14-6501-2014, 2014.

Watson, L. , Lacressonnière, G., Gauss, M., Engardt, M., Andersson, C., Josse, B., Marécal, V., Nyiri, A., Sobolowski, S., Siour, G., Szopa, S., Vautard, R.: The impact of emissions and +2∘ C climate change upon future ozone and nitrogen dioxide over Europe, Atmos. Env., 142, 271-285, 2016.

Wennberg, P. O., Cohen, R. C., Stimpfle, R. M., Koplow, J. P., Anderson, J. G., Salawitch, R. J., Fahey, D. W., Woodbridge, E. L., Keim,
5   E. R., Gao, R. S., Webster, C. R., May, R. D., Toohey, D., Avallone, L., Proffitt, M. H., Loewenstein, M., Podolske, J. R., Chan, K. R., and Wofsy, S. C.: Removal of stratospheric O_3 by radicals: in situ measurements of OH, HO2 , NO, NO_2, ClO and BrO, Science, 266, 398–404, 1994.

Whitten, G. Z., Hogo, H., and Killus, J. P.: The Carbon-Bond Mechanism : A Condensed Kinetic Mechanism for Photochemical Smog, Environ. Sci., 14 (6), 690–700, doi: 10.1021/es60166a008, 1980.

10 Wiedinmyer, C., Akagi, S. K., Yokelson, R. J., Emmons, L. K., Al-Saadi, J. A., Orlando, J. J., and Soja, A. J.: The Fire INventory from NCAR (FINN): a high resolution global model to estimate the emissions from open burning, Geosci. Model Dev., 4, 625-641, doi:10.5194/gmd-4-625-2011, 2011.

Wittrock, F., Oetjen, H., Richter, A., Fietkau, S., Medeke, T., Rozanov, A., and Burrows, J. P.: MAX-DOAS measurements of atmospheric trace gases in Ny-Ålesund - Radiative transfer studies and their application, Atmos. Chem. Phys., 4, 955-966, 2004.

15 Wittrock, F.: The retrieval of oxygenated volatile organic compounds by remote sensing techniques, Ph.D., University of Bremen, Bremen, Germany, available at: http://www.doas-bremen.de/paper/diss wittrock 06.pdf, 2006.

Zien, A. W., Richter, A., Hilboll, A., Blechschmidt, A.-M., and Burrows, J. P.: Systematic analysis of tropospheric NO_2 long-range transport events detected in GOME-2 satellite data, Atmos. Chem. Phys., 14, 7367-7396, doi:10.5194/acp-14-7367-2014, 2014.

Zyryanov, D., Foret, G., Eremenko, M., Beekmann, M., Cammas, J.-P., D'Isidoro, M., Elbern, H., Flemming, J., Friese, E., Kioutsioutkis,
20 I., Maurizi, A., Melas, D., Meleux, F., Menut, L., Moinat, P., Peuch, V.-H., Poupkou, A., Razinger, M., Schultz, M., Stein, O., Suttie, A. M., Valdebenito, A., Zerefos, C., Dufour, G., Bergametti, G., and Flaud, J.-M.: 3-D evaluation of tropospheric ozone simulations by an ensemble of regional Chemistry Transport Model, Atmos. Chem. Phys., 12, 3219–3240, doi:10.5194/acp-12-3219-2012, 2012.
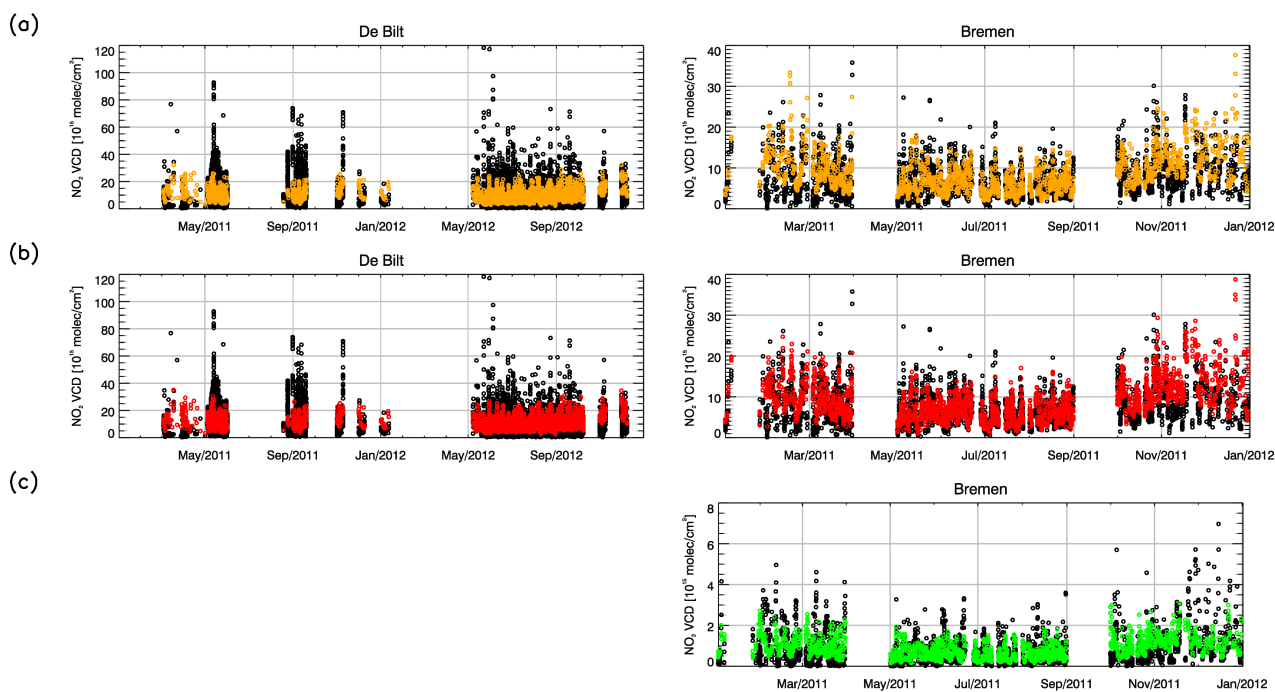
Figure 1. Time series of tropospheric NO_2 VCDs [10^{15} molec cm^{-2}] calculated by (a) method 1, (b) method 2 and (c) surface partial columns [10^{15} molec cm^{-2}] from (black circles) MAX-DOAS and (colored circles) model ensemble hourly data for (left) De Bilt and (right) Bremen. Surface partial columns from MAX-DOAS are not available for De Bilt for the investigated time period.

Atmospheric
Chemistry
and Physics
Discussions
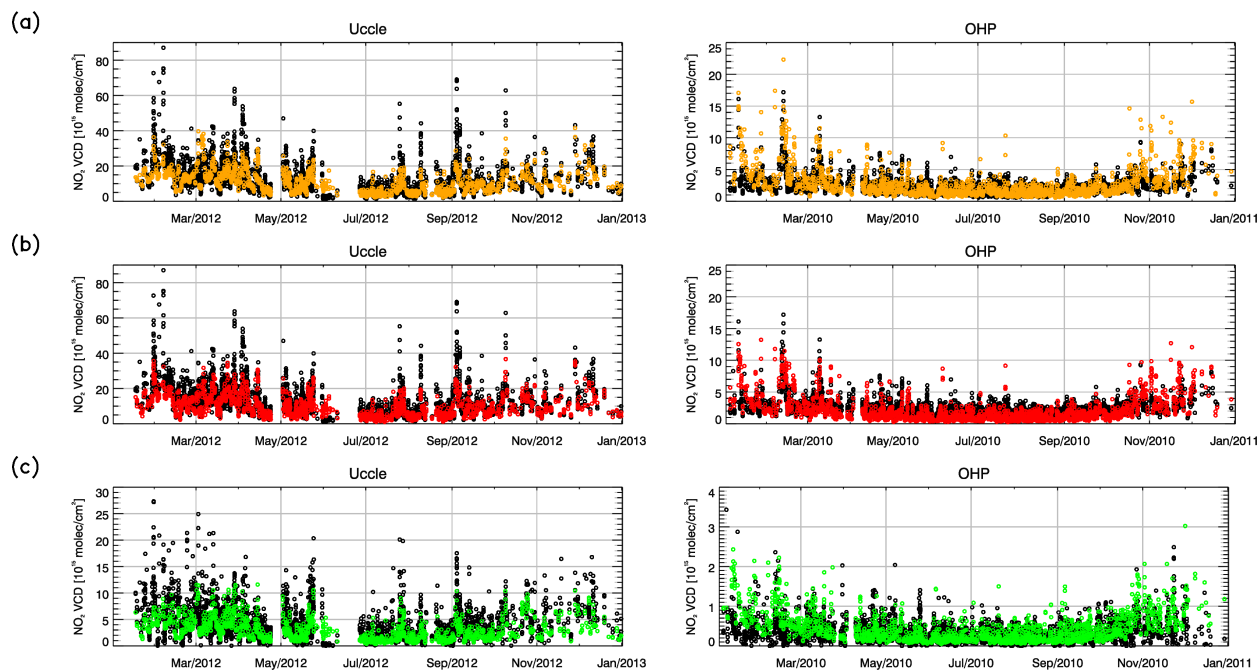
Figure 2. As in Figure 1 but for (left) Uccle and (right) OHP.
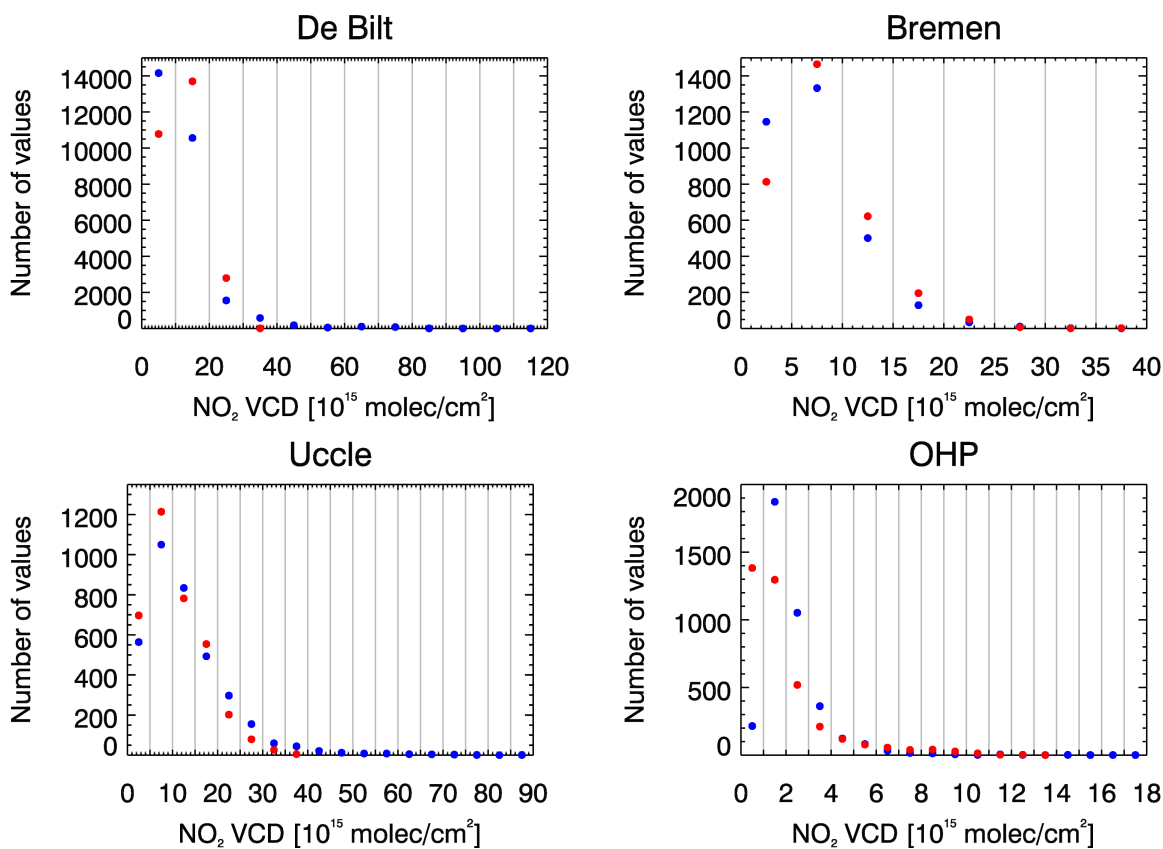
Figure 3. Frequency distributions of tropospheric NO_2 VCDs [10^{15} molec cm^{-2}] for (blue) MAX-DOAS and (red) model ensemble data from method 2 for (top left) De Bilt, (top right) Bremen, (lower left) Uccle and (lower right) OHP. The size of the bins used to calculate the number of values given on the y-axis is shown by vertical grey lines.
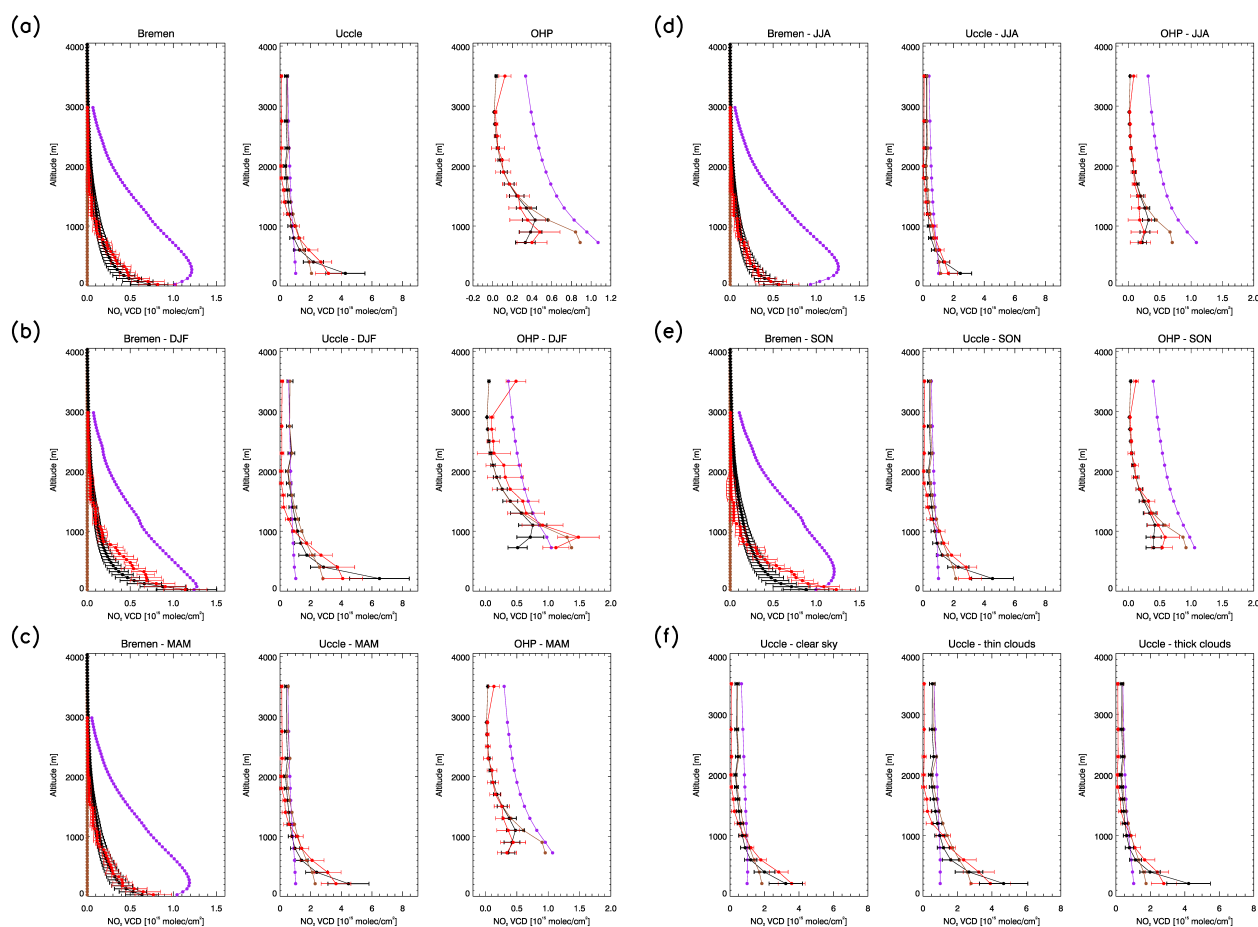
Figure 4. Vertical profiles of NO$_2$ partial columns [10^{15} molec cm^{-2}] from (black) MAX-DOAS, (brown) a priori used for MAX-DOAS retrievals, (purple) column averaging kernels and (red) model ensemble data. Red error bars show the standard deviation of the model ensemble based on all separate model runs. Black error bars refer to the uncertainty associated with the MAX-DOAS retrievals (assumed to be 30 % for all stations). Panel (a) shows profiles for data averaged over whole time series, panel (b) shows profiles for DJF (December, January February), (c) MAM (March, April, May), (d) JJA (June, July, August) and (e) SON (September, October, November) months only. Figures in panels (a) to (e) refer to (left) Bremen, (middle) Uccle and (right) OHP. Figures in panel (f) correspond to (left) clear-sky, (middle) thin cloud and (right) thick cloud conditions for station Uccle only. MAX-DOAS vertical profiles are not available for De Bilt for the investigated time period.

Atmospheric
Chemistry
and Physics
Discussions
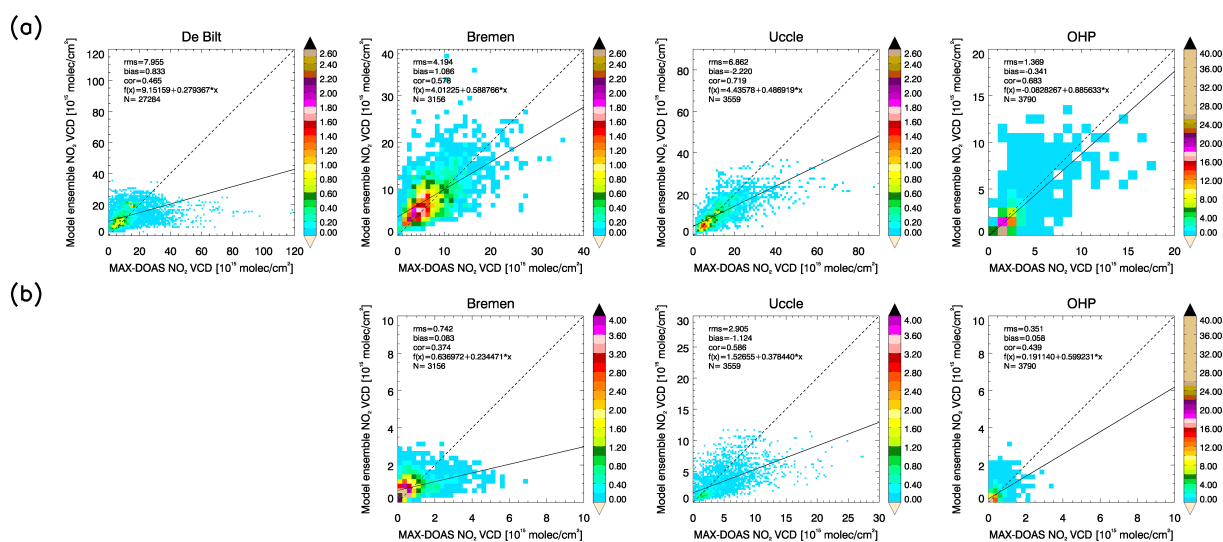
Figure 5. Scatter density plots of (a) tropospheric NO_2 VCDs [10^{15} molec cm^{-2}] calculated by method 2 and (b) surface partial columns [10^{15} molec cm^{-2}] for (from left to right) De Bilt, Bremen, Uccle and OHP. The data is shown for different bins with a size of 10^{15} molec cm^{-2} and is colored according to the number of data points per bin [%]. The dashed line is the reference line (f(x)=x). The solid line is the regression line (see top left of each plot for f(x) of this line). The root mean squared error (rms) [10^{15} molec cm^{-2}], bias [10^{15} molec cm^{-2}], correlation coefficient (cor, not squared) as well as the number of data points N are given at the top left of each plot. Surface partial columns from MAX-DOAS are not available for De Bilt for the investigated time period.
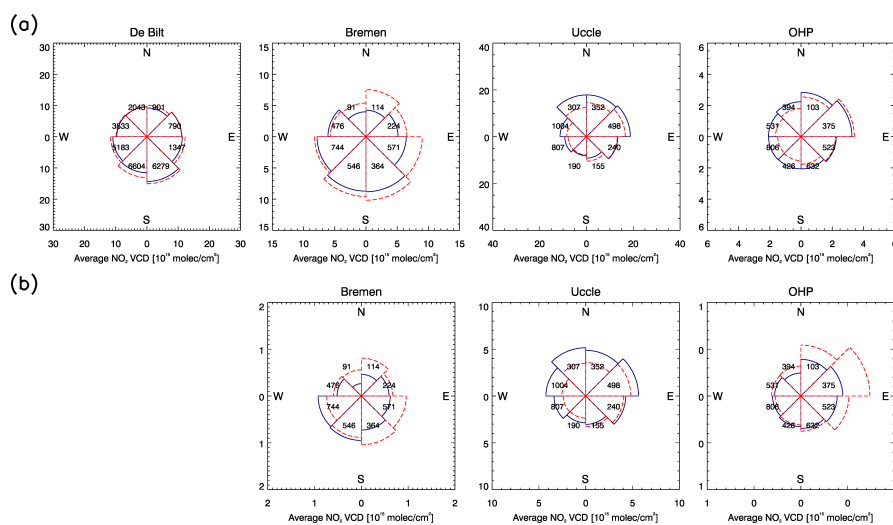
Figure 6. (a) Average tropospheric NO$_2$ VCDs [10^{15} molec cm^{-2}] calculated by method 2 and (b) average surface partial columns [10^{15} molec cm^{-2}], both in 45° wide wind direction bins from (blue solid lines) MAX-DOAS and (red dashed lines) model ensemble data for (from left to right) De Bilt, Bremen, Uccle and OHP. Wind directions correspond to the direction towards the station and are taken from weather station measurements. The numbers close to the centre of each plot refer to the data values used for calculating average values for each bin. Surface partial columns from MAX-DOAS are not available for De Bilt for the investigated time period.
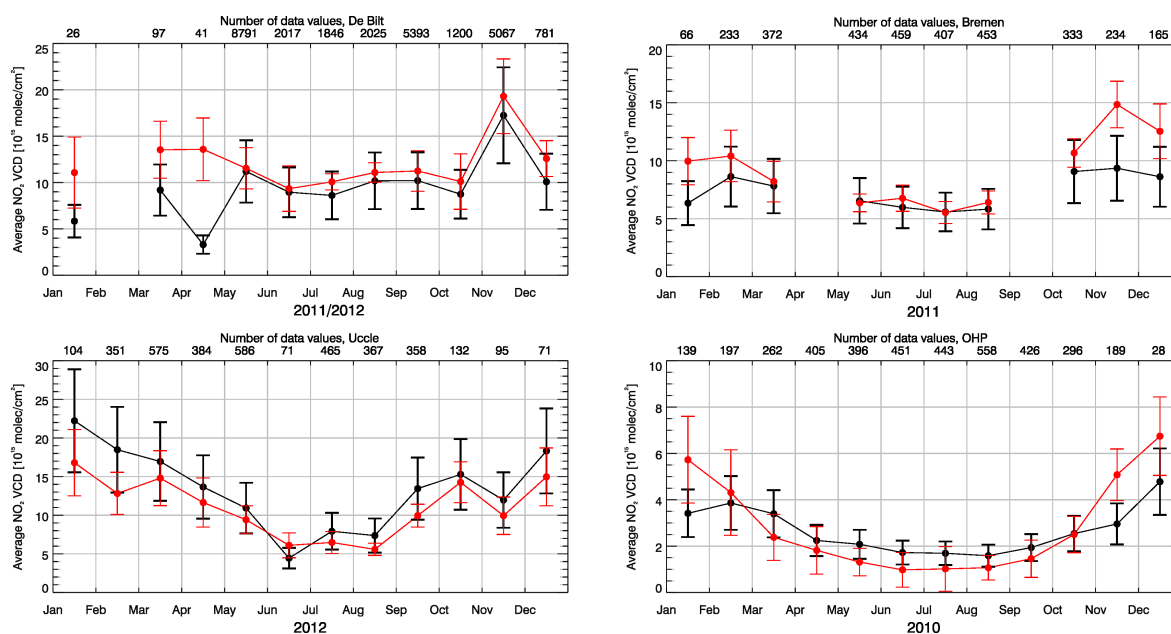
Figure 7. Seasonal cycles (monthly averages) of tropospheric NO_2 VCDs [10^{15} molec cm^{-2}] from (black) MAX-DOAS and (red) model ensemble data from method 2 for (top left) De Bilt, (top right) Bremen, (lower left) Uccle and (lower right) OHP. Red error bars show the standard deviation of the model ensemble based on all separate model runs. Black error bars refer to the uncertainty associated with the MAX-DOAS retrievals (assumed to be 30 % for all stations). The number of data values used for calculating average values is shown at the upper x-axis of each plot.
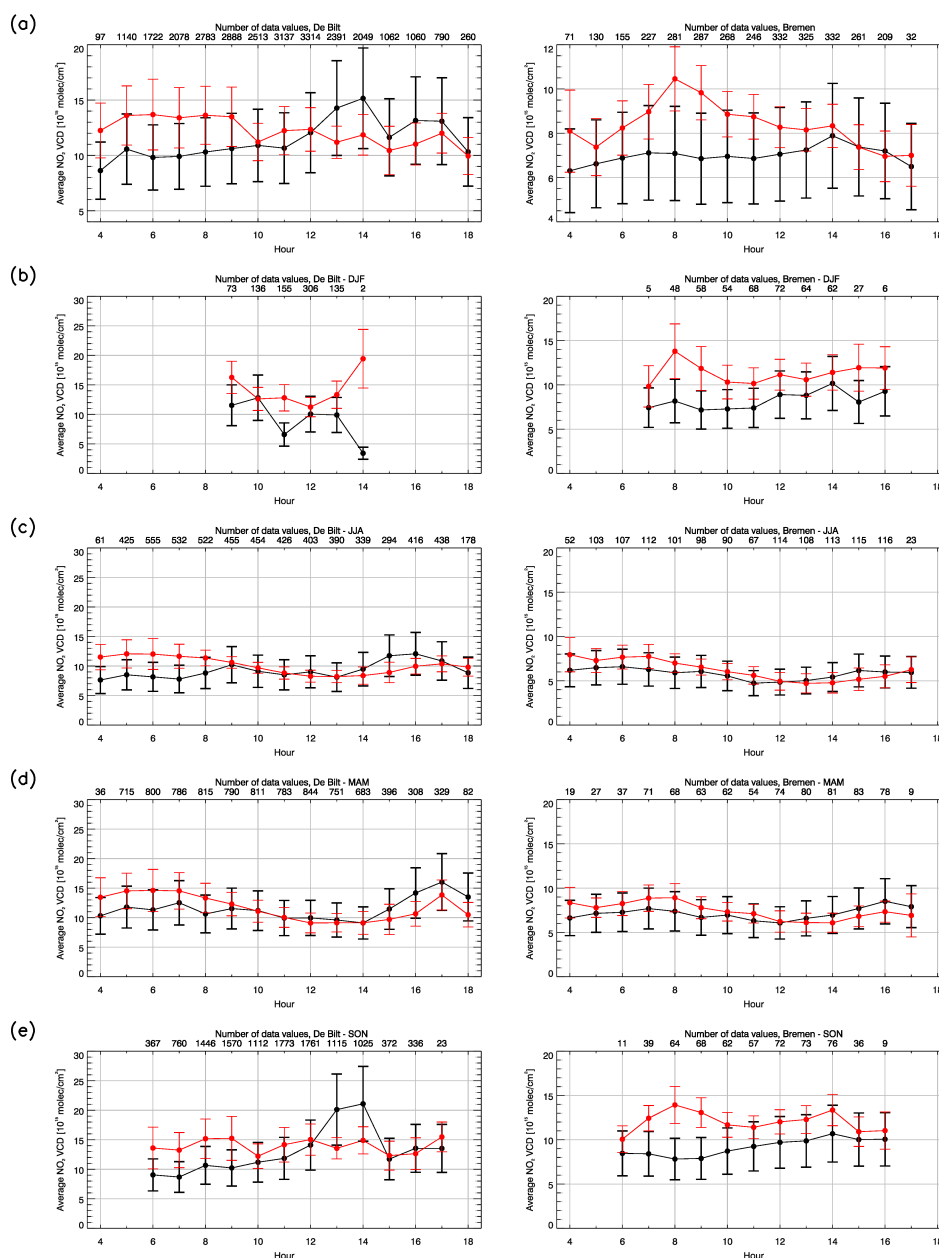
Figure 8. Diurnal cycles (averages over hourly bins) of tropospheric NO_2 VCDs [10^{15} molec cm^{-2}] from (black) MAX-DOAS and (red) model ensemble data from method 2 for (left) De Bilt and (right) Bremen. Red error bars show the standard deviation of the model ensemble based on all separate model runs. Black error bars refer to the uncertainty associated with the MAX-DOAS retrievals (assumed to be 30 % for all stations). Panel (a) shows cycles for the whole time series, panel (b) shows cycles for DJF, (c) MAM, (d) JJA and (e) SON months only. The number of data values used for calculating average values is shown at the top x-axis of each plot.
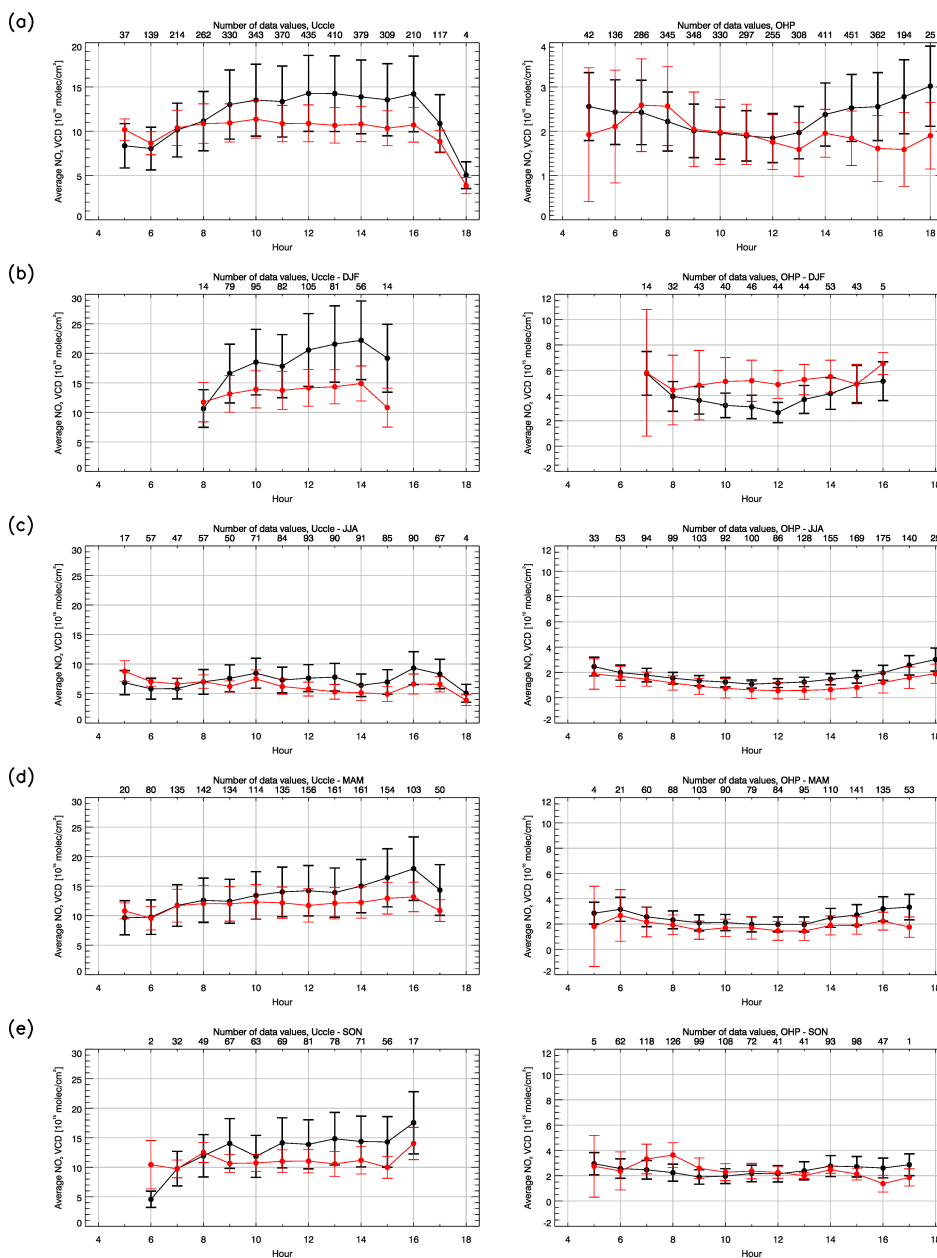
Figure 9. As in Figure 8 but for (left) Uccle and (right) OHP.
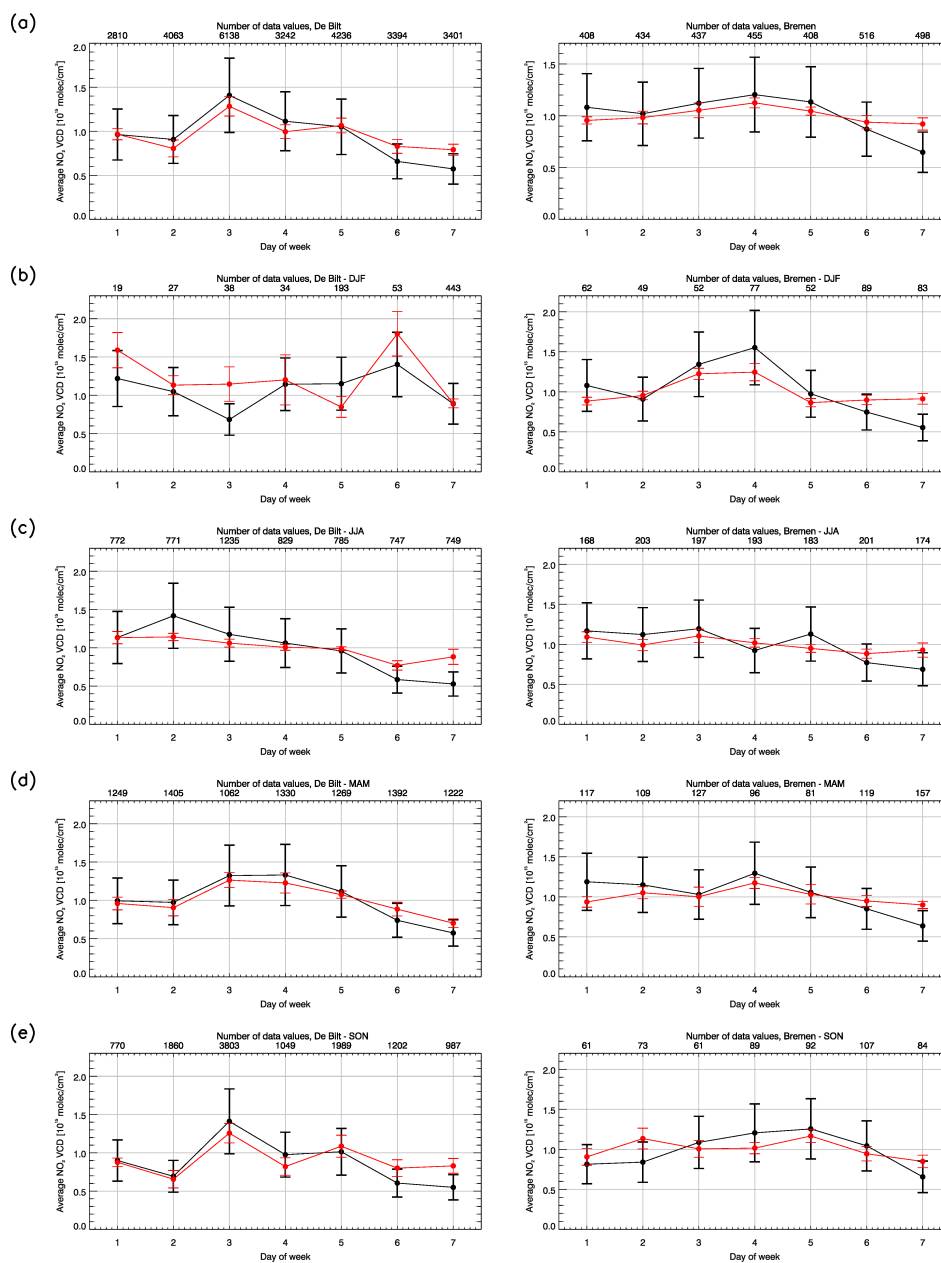
Figure 10. Weekly cycles (averages over daily bins devided by mean over whole week) of tropospheric NO$_2$ VCDs [10^{15} molec cm^{-2}] calculated by method 2 from (black) MAX-DOAS and (red) model ensemble data for (left) De Bilt and (right) Bremen. Day of week number 1 to 7 refers to Monday to Sunday, respectively. Red error bars show the standard deviation of the model ensemble based on all separate model runs. Black error bars refer to the uncertainty associated with the MAX-DOAS retrievals (assumed to be 30 % for all stations). Panel (a) shows cycles for the whole time series, panel (b) shows cycles for DJF, (c) MAM, (d) JJA and (e) SON months only. The number of data values used for calculating average values is shown at the top x-axis of each plot.

Atmospheric
Chemistry
and Physics
Discussions
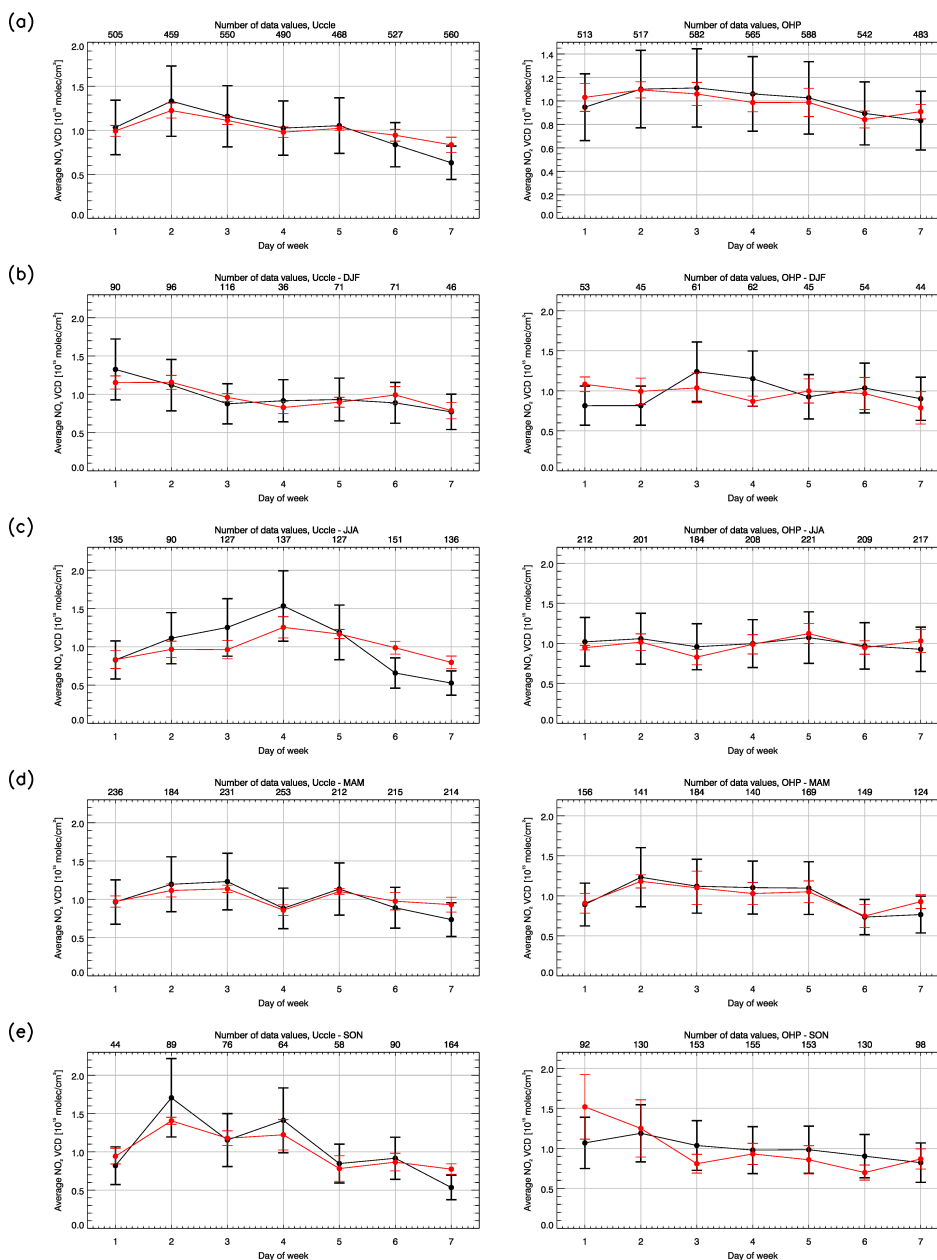
Figure 11. As in Figure 10 but for (left) Uccle and (right) OHP.

Atmospheric
Chemistry
and Physics
Discussions

Table 1. Overview of regional air quality model simulations.

Model	Institution	Horizontal grid spacing (zonal x meridional)	Number of vertical levels/model top	Chemistry scheme
CHIMERE	LISA-CNRS/UPEC/UPD, INERIS	0.25 x 0.25 deg ($\sim$ 18 x 28 km)	8/ 500 hPa	MELCHIOR II (Schmidt et al., 2001)
EMEP-MACCEVA	MetNo	0.25 x 0.125 deg ($\sim$ 18 x 14 km)	20/ 100 hPa	EMEP-EmChem09soa (Simpson et al., 2012; Bergström et al., 2012)
EMEP	MetNo	50 x 50 km	20/ 100 hPa	EMEP-EmChem09soa (Simpson et al., 2012; Bergström et al., 2012)
LOTOS-EUROS	TNO	0.125 x 0.0625 deg ($\sim$ 9 x 7 km)	3/ $\sim$ 3.5 km	TNO CBM-IV (Schaap et al., 2008; Whitten et al., 1980)
MOCAGE	CNRS-Météo-France	0.2 x 0.2 deg ($\sim$ 15 x 22 km)	47/ 5 hPa	troposphere: RACM (Stockwell et al., 1997), stratosphere: REPROBUS (Lefèvre et al., 1994)
SILAM	FMI	years 2010/2011: 0.2 x 0.2 deg ($\sim$ 15 x 22 km); year 2012: 0.15 x 0.15 deg ($\sim$ 11 x 17 km)	9 (2010), 8 (2011-2012)/ 6.725 km (2010), 6.7 km (2011-2012)	DMAT (Sofiev, 2000)

Atmospheric
Chemistry
and Physics
Discussions

Table 2. Overview of MAX-DOAS station data.

Station, country	Latitude, longitude, station height above sea level	Institution	Time period	Characterisation	Retrieved quantity	number of measurement layers, top layer altitude	additional data
De Bilt, Netherlands	52.1° N, 5.18° E, ∼ 23 m	KNMI	March 2011 – Dec 2012	urban	column	12, 4.0 km	wind data (in-situ)
Bremen, Germany	53.11° N, 8.86° E, ∼ 21 m	IUP-UB	Jan – Dec 2011	urban	column/ profile	81, 4.025 km	wind data (in-situ data from airport weather station ∼ 9 km southwards at 53.05° N, 8.79° E)
Uccle, Belgium	50.8° N, 4.32° E, 120 m	BIRA-IASB	Jan – Dec 2012	urban	column/ profile	13, 3.5 km	wind data (in-situ), clouds from MAX-DOAS
OHP, France	43.92° N, 5.7° E, 650 m	BIRA-IASB	Jan – Dec 2010	rural	column/ profile	13, 3.5 km	wind data (in-situ)

Atmospheric
Chemistry
and Physics
Discussions

Open Access

EGU

Appendix A: Appendix
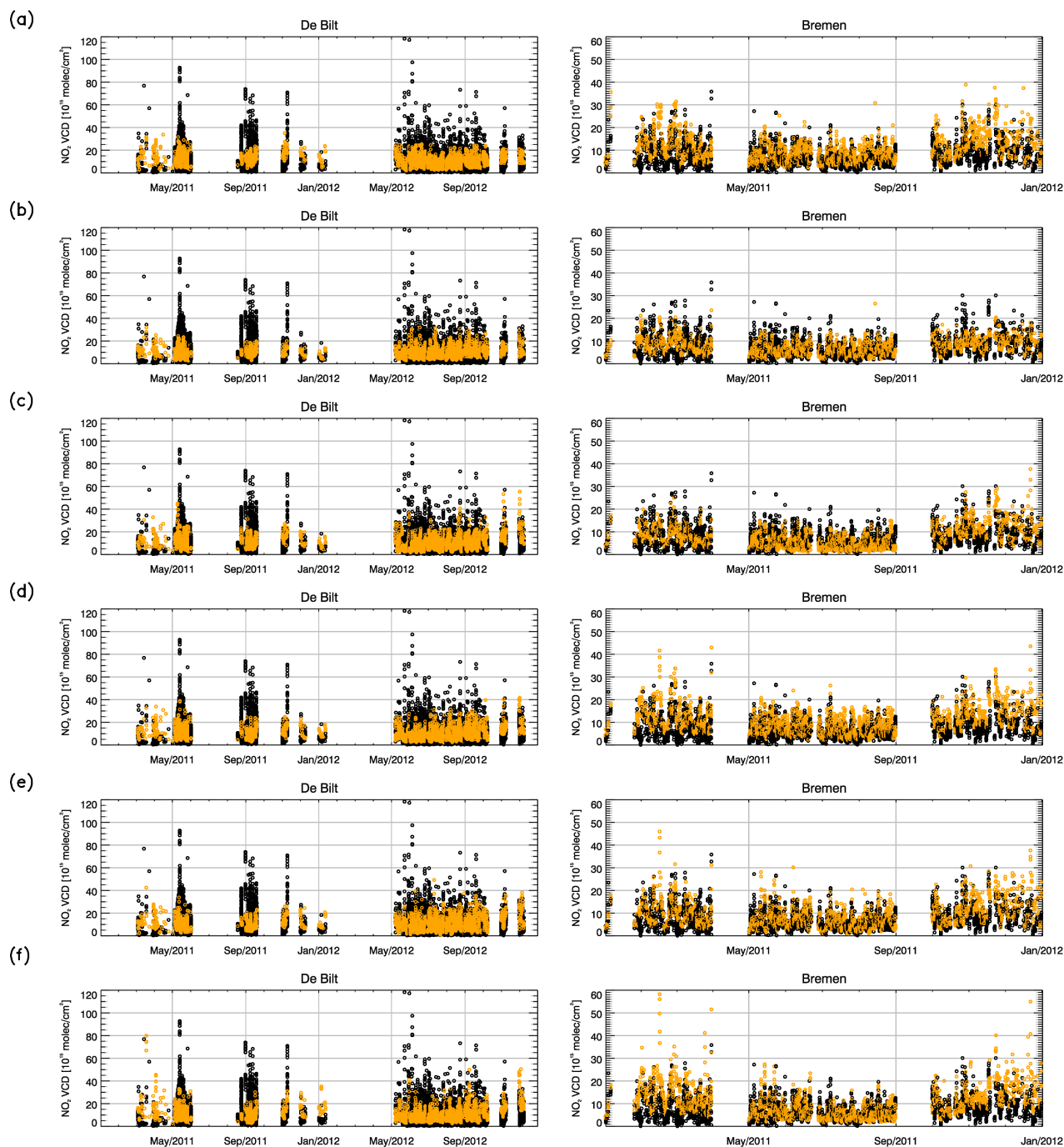
Figure A1. Time series of tropospheric NO_2 VCDs [10^{15} molec cm^{-2}] from (black circles) MAX-DOAS and (colored circles) model data calculated using method 1 for (left) De Bilt and (right) Bremen. The different panels show different model runs: (a) LOTOS-EUROS, (b) CHIMERE, (c) EMEP, (d) EMEP-MACCEVA, (e) SILAM and (f) MOCAGE.

Atmospheric
Chemistry
and Physics
Discussions
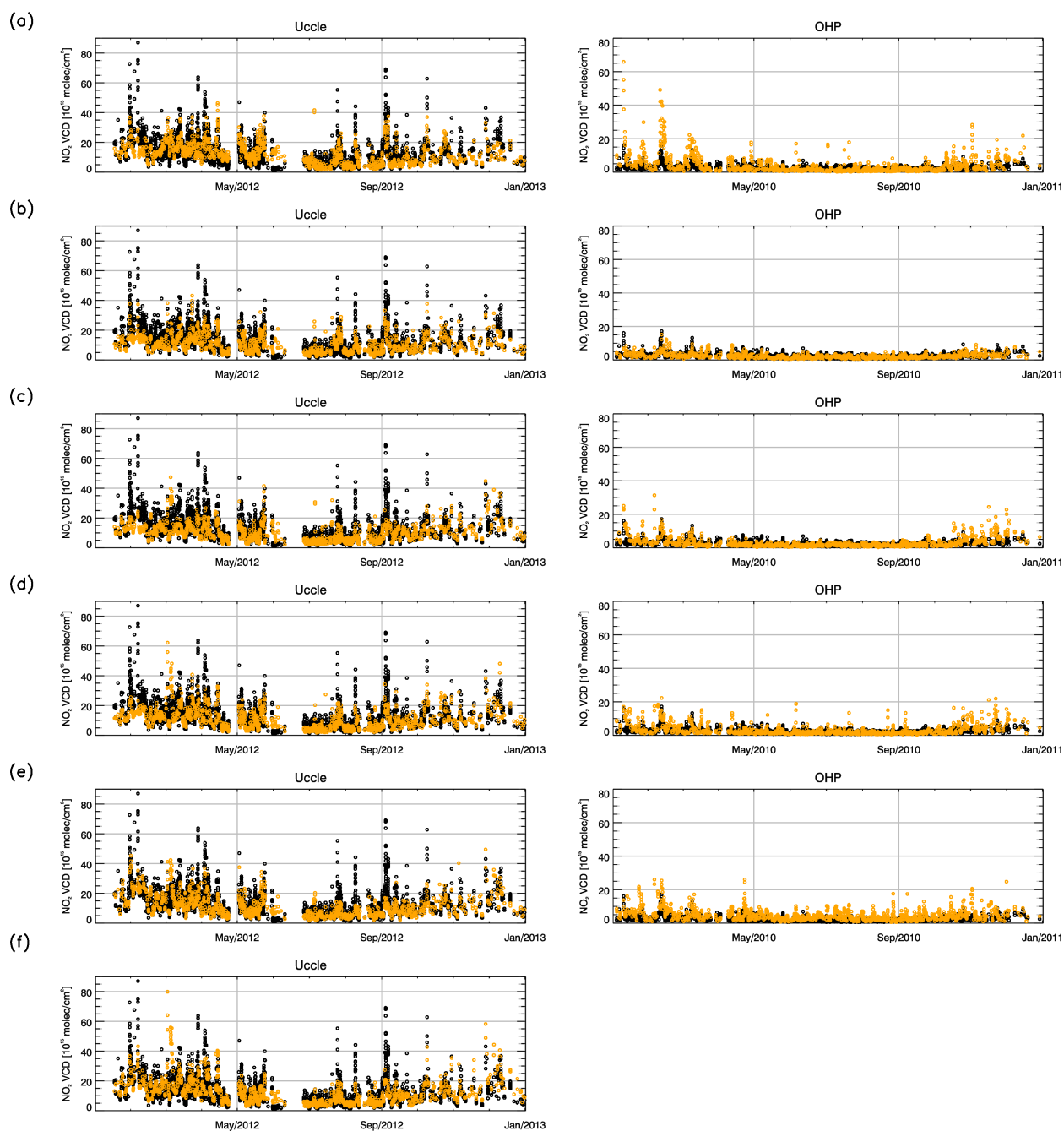
Figure A2. As in Figure A1 but for (left) Uccle and (right) OHP. MOCAGE data is not available for the measurement time period at OHP.
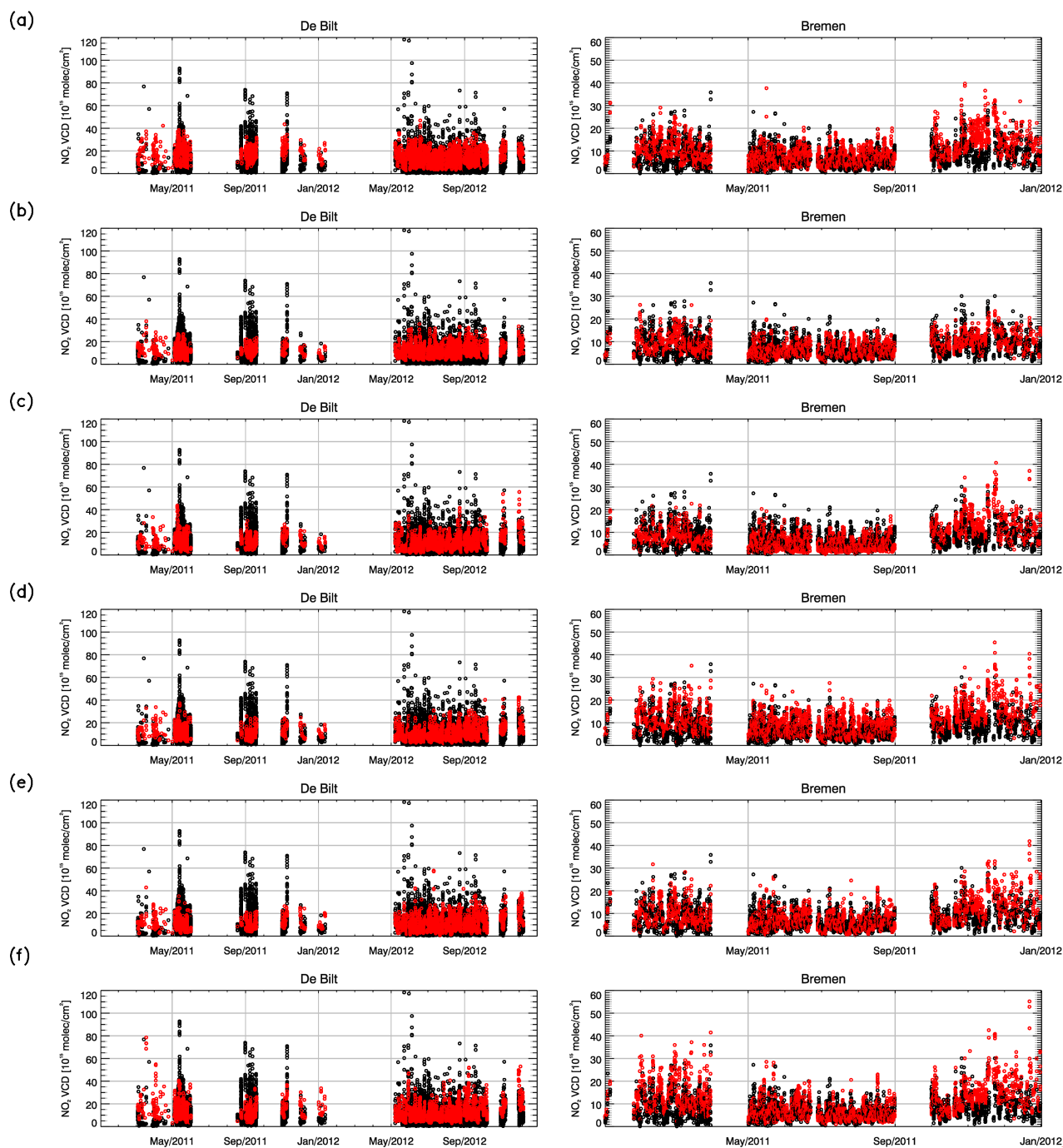
Figure A3. As in Figure A1 but for model data calculated using method 2.
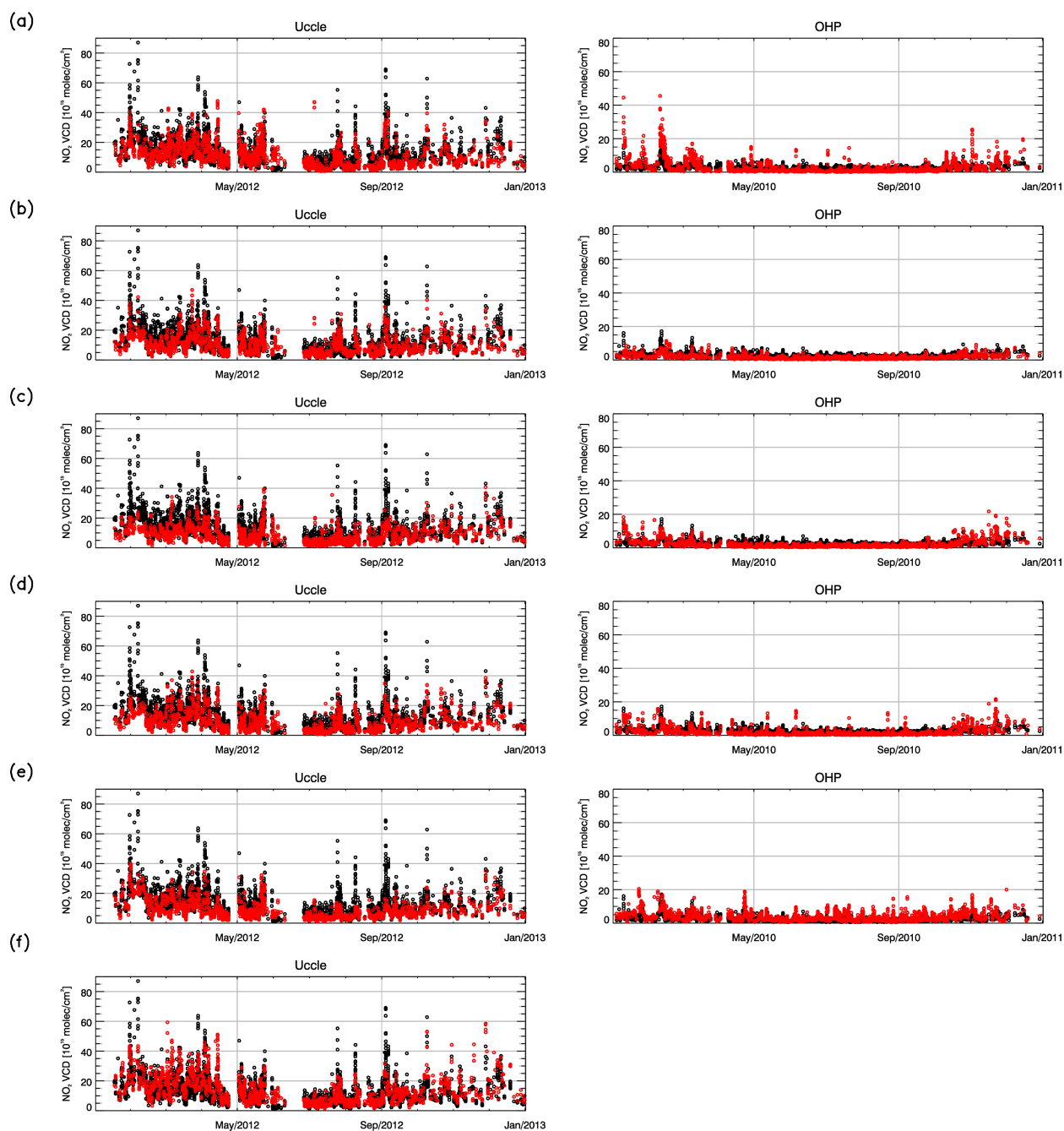
Figure A4. As in Figure A2 but for model data calculated using method 2.
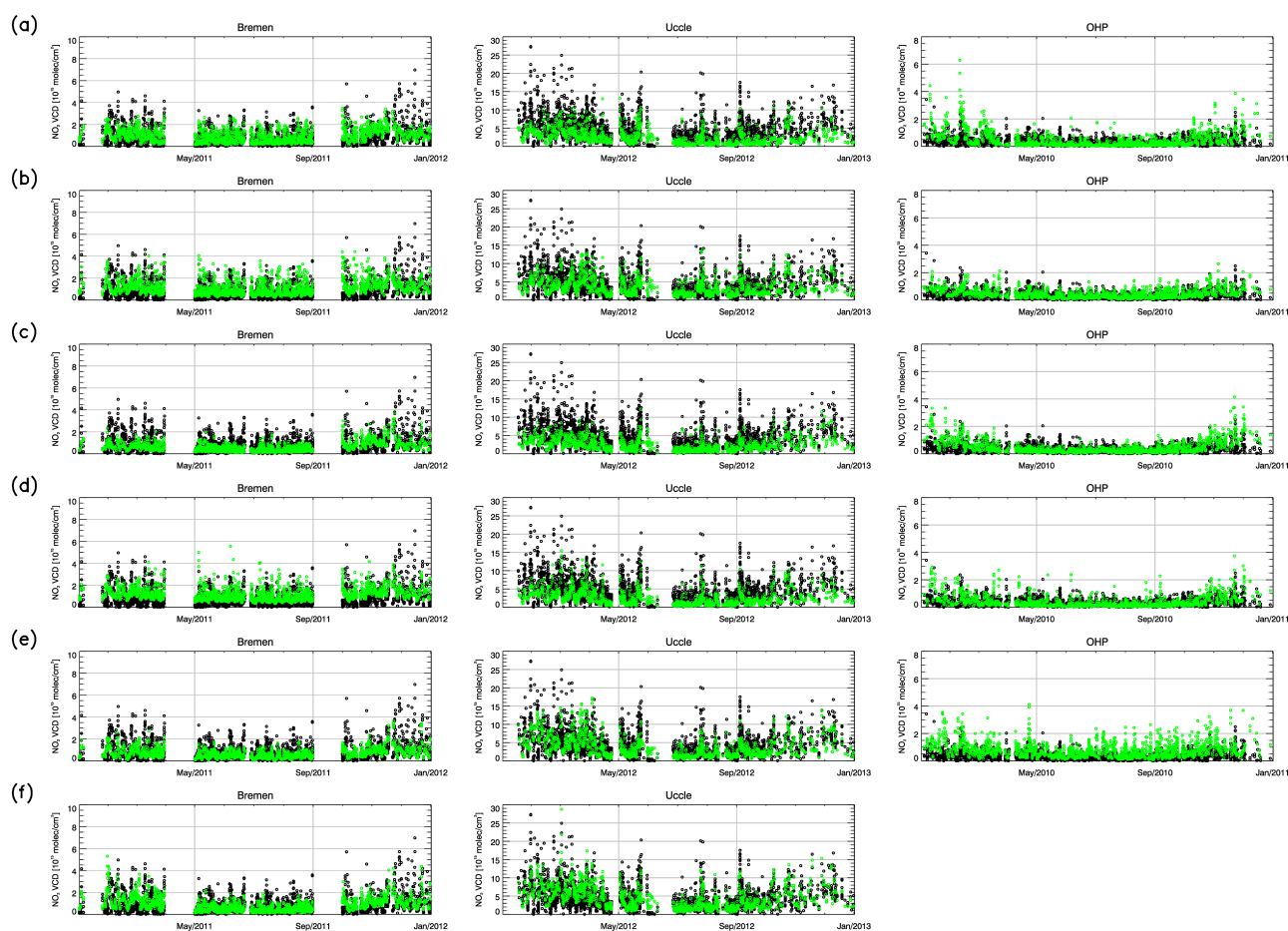
Figure A5. Time series of surface partial columns of tropospheric NO_2 VCDs [10^{15} molec cm^{-2}] from (black circles) MAX-DOAS and (colored circles) model data for (left) Bremen, (middle) Uccle and (right) OHP. The different panels show different model runs: (a) LOTOS-EUROS, (b) CHIMERE, (c) EMEP, (d) EMEP-MACCEVA, (e) SILAM and (f) MOCAGE. Surface partial columns from MAX-DOAS for De Bilt and MOCAGE data for OHP are not available for the corresponding measurement time periods.

Atmospheric
Chemistry
and Physics
Discussions
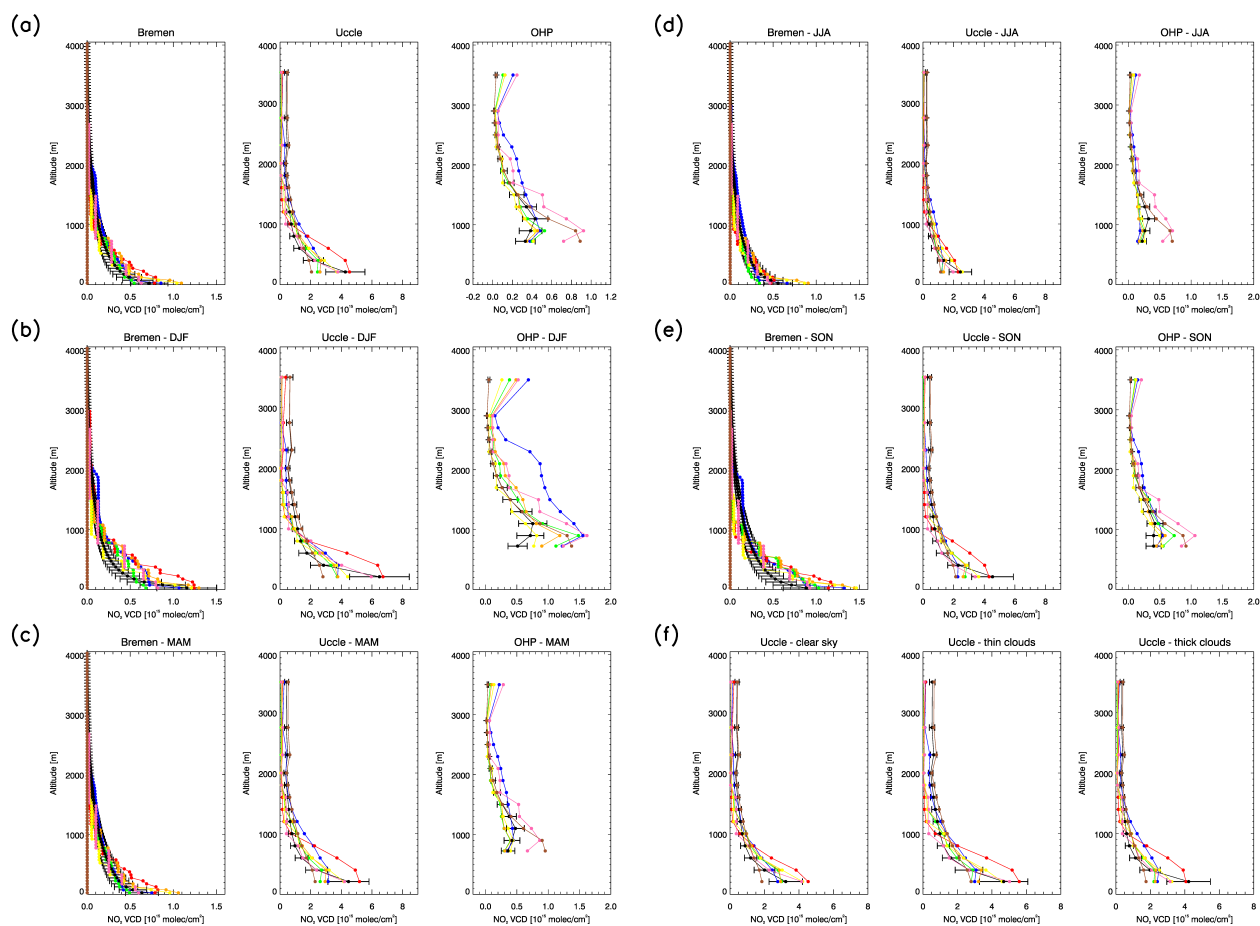
Figure A6. As in Figure 4 but for separate model runs: (blue) LOTOS-EUROS, (yellow) CHIMERE, (green) EMEP, (orange) EMEP-MACCEVA, (pink) SILAM and (red) MOCAGE. MAX-DOAS vertical profiles are not available for De Bilt for the investigated time period.
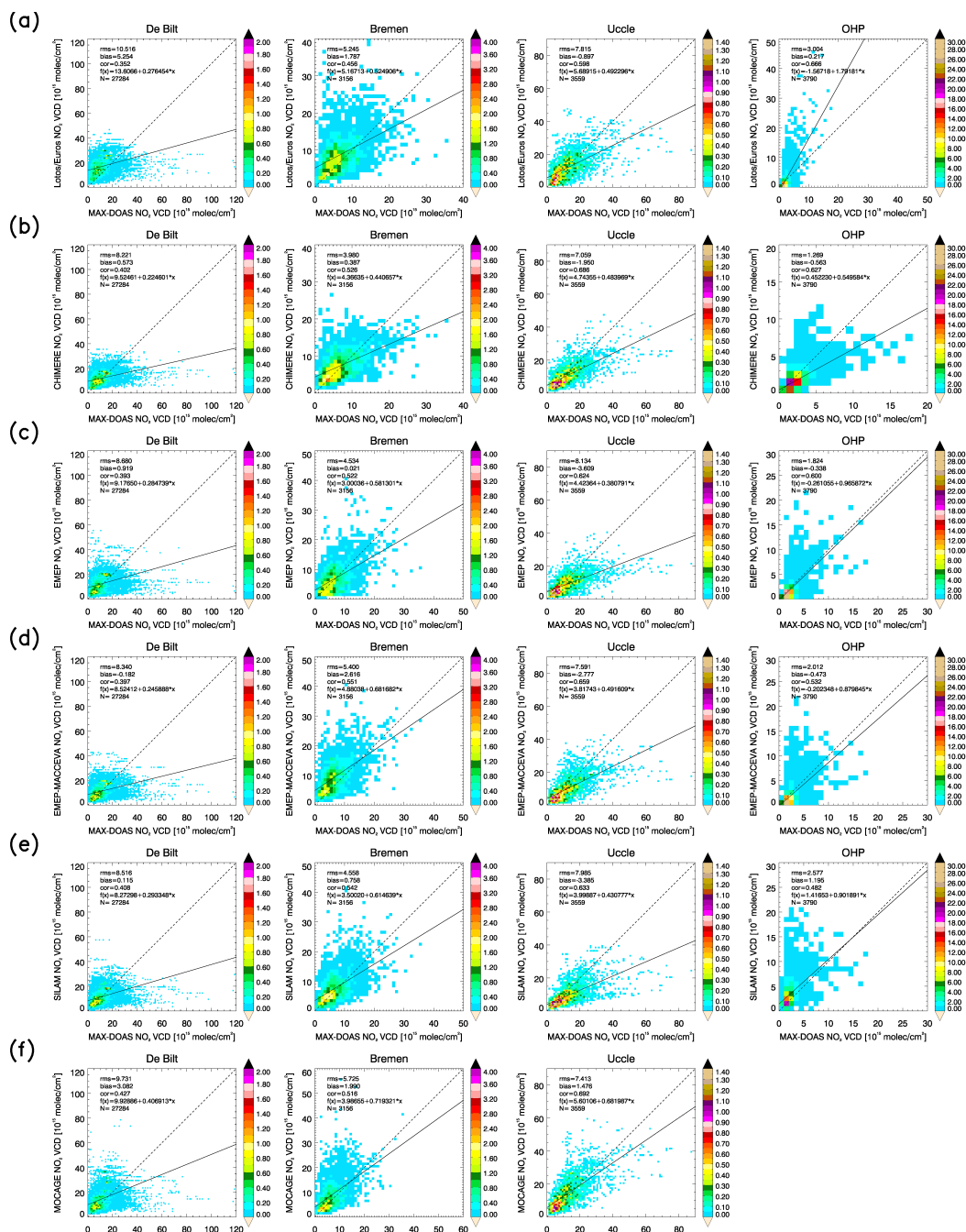
Figure A7. Scatter density plots of tropospheric NO_2 VCDs [10^{15} molec cm^{-2}] from MAX-DOAS against model data from method 2 for (from left to right) De Bilt, Bremen, Uccle and OHP. The data is shown for different bins with a size of 10^{15} molec cm^{-2} and is colored according to the number of data points per bin [%]. The different panels show different model runs: (a) LOTOS-EUROS, (b) CHIMERE, (c) EMEP, (d) EMEP-MACCEVA, (e) SILAM and (f) MOCAGE. MOCAGE data is not available for the measurement time period at OHP.
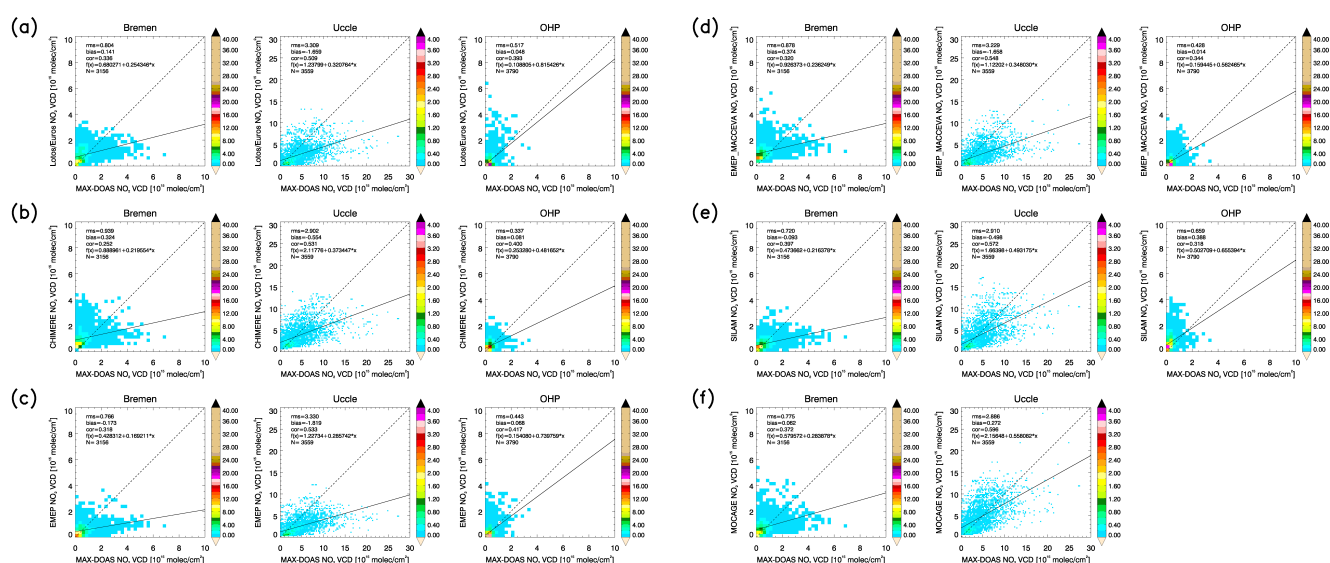
Figure A8. Scatter density plots of surface partial columns of tropospheric NO_2 VCDs [10^{15} molec cm^{-2}] from MAX-DOAS against model data for (left) Bremen, (middle) Uccle and (right) OHP. The data is shown for different bins with a size of 10^{15} molec cm^{-2} and is colored according to the number of data points per bin [%]. The different panels show different model runs: (a) LOTOS-EUROS, (b) CHIMERE, (c) EMEP, (d) EMEP-MACCEVA, (e) SILAM and (f) MOCAGE. Surface partial columns from MAX-DOAS for De Bilt and MOCAGE data for OHP are not available for the corresponding measurement time periods.

Atmospheric
Chemistry
and Physics
Discussions

Open Access
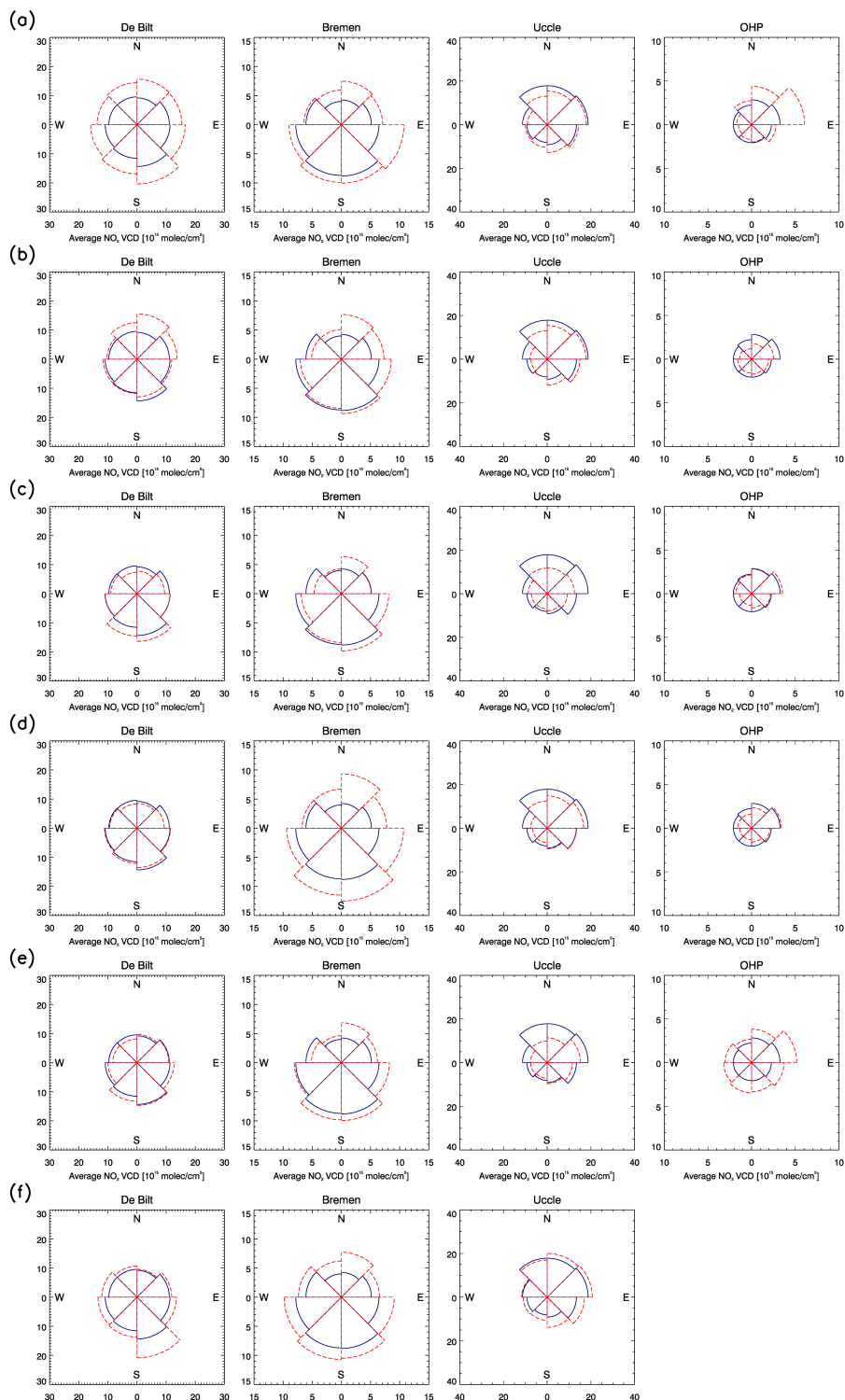
Figure A9. As in Figure A7 but for average tropospheric NO$_2$ VCDs [10^{15} molec cm^{-2}] in 45° wide wind direction bins from (blue solid lines) MAX-DOAS and (red dashed lines) model data. MOCAGE data is not available for the measurement time period at OHP.
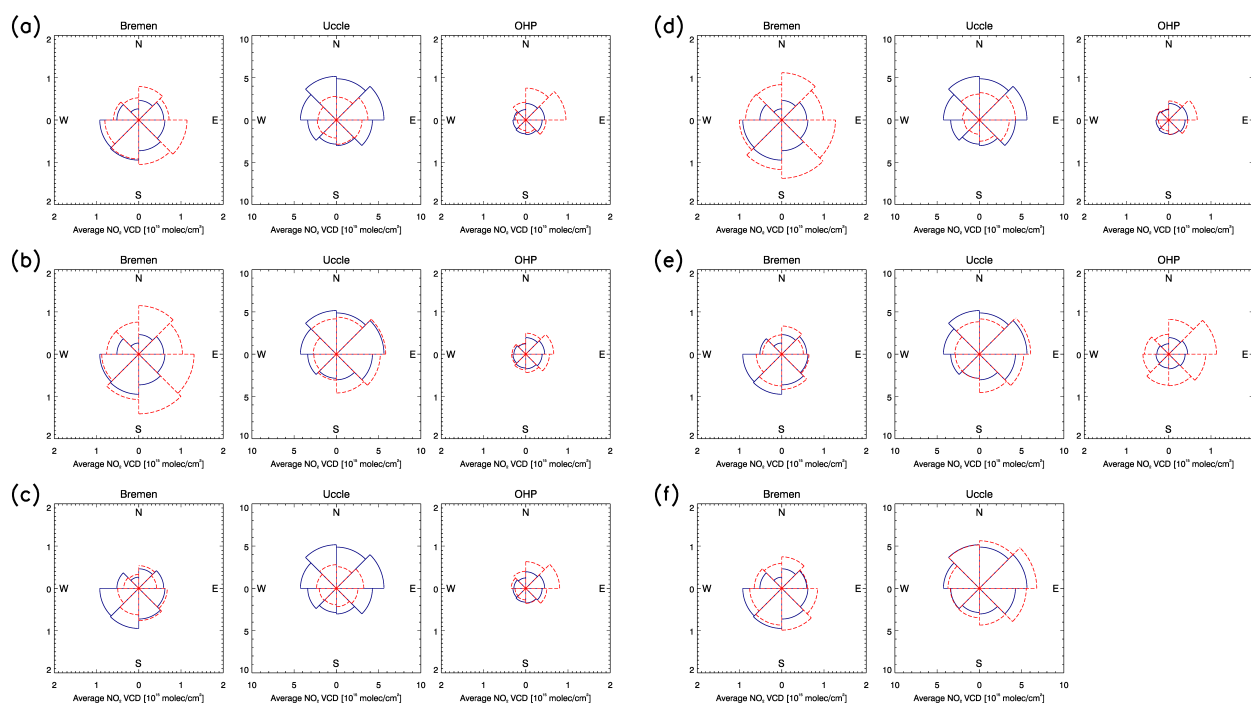
Figure A10. As in Figure A8 but for average tropospheric NO_2 VCDs [10^{15} molec cm^{-2}] in 45° wide wind direction bins from (blue solid lines) MAX-DOAS and (red dashed lines) model data. Surface partial columns from MAX-DOAS for De Bilt and MOCAGE data for OHP are not available for the corresponding measurement time periods.

Atmospheric
Chemistry
and Physics
Discussions
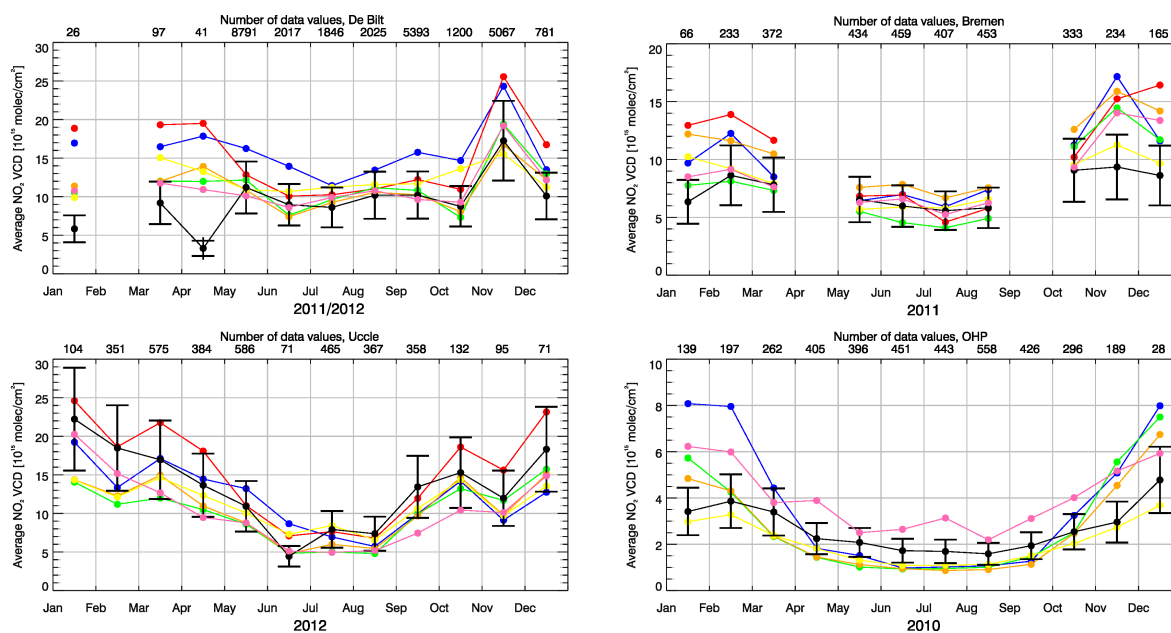
Figure A11. As in Figure 7 but for separate model runs: (blue) LOTOS-EUROS, (yellow) CHIMERE, (green) EMEP, (orange) EMEP-MACCEVA, (pink) SILAM and (red) MOCAGE.
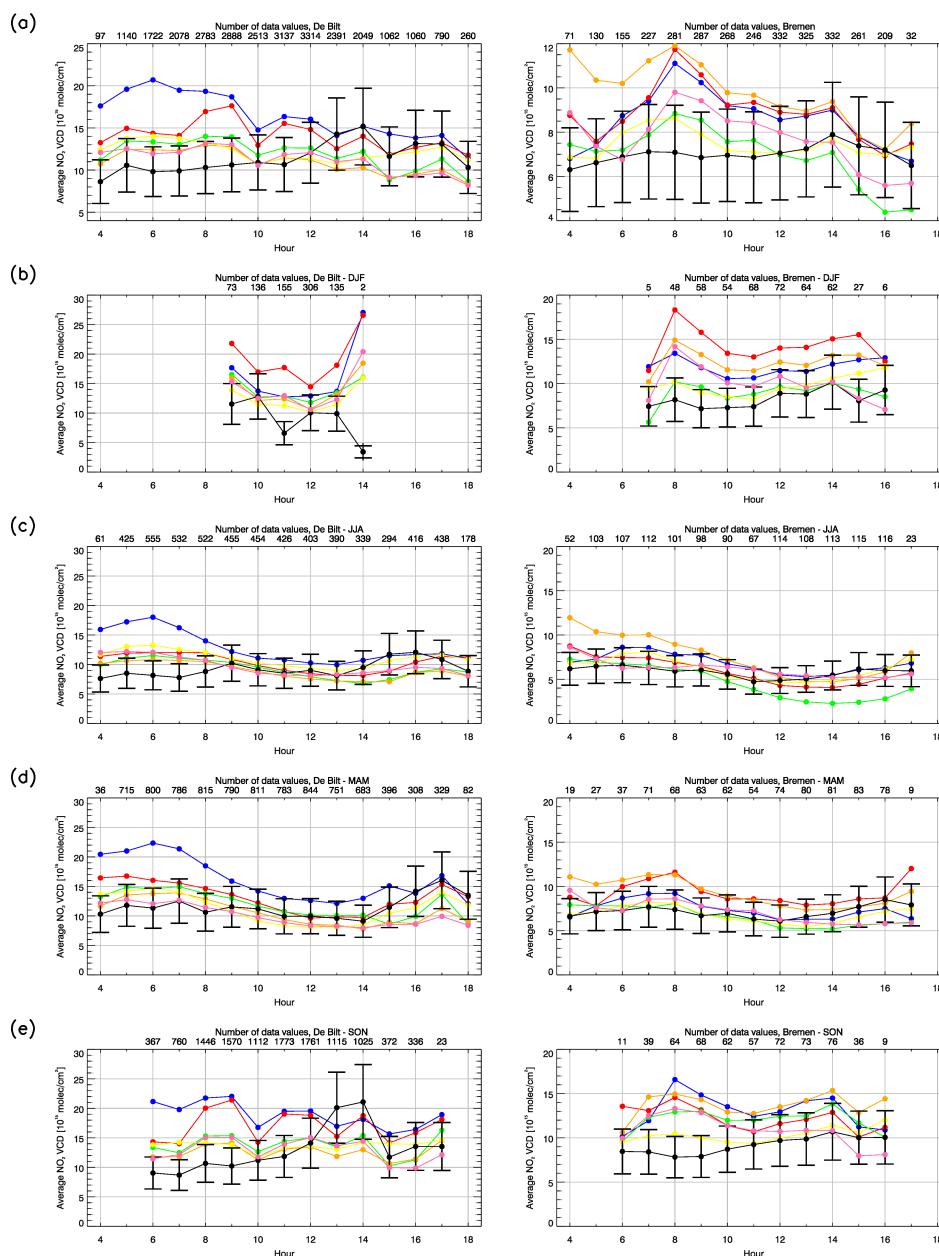
Figure A12. As in Figure 8 but for separate model runs: (blue) LOTOS-EUROS, (yellow) CHIMERE, (green) EMEP, (orange) EMEP-MACCEVA, (pink) SILAM and (red) MOCAGE.
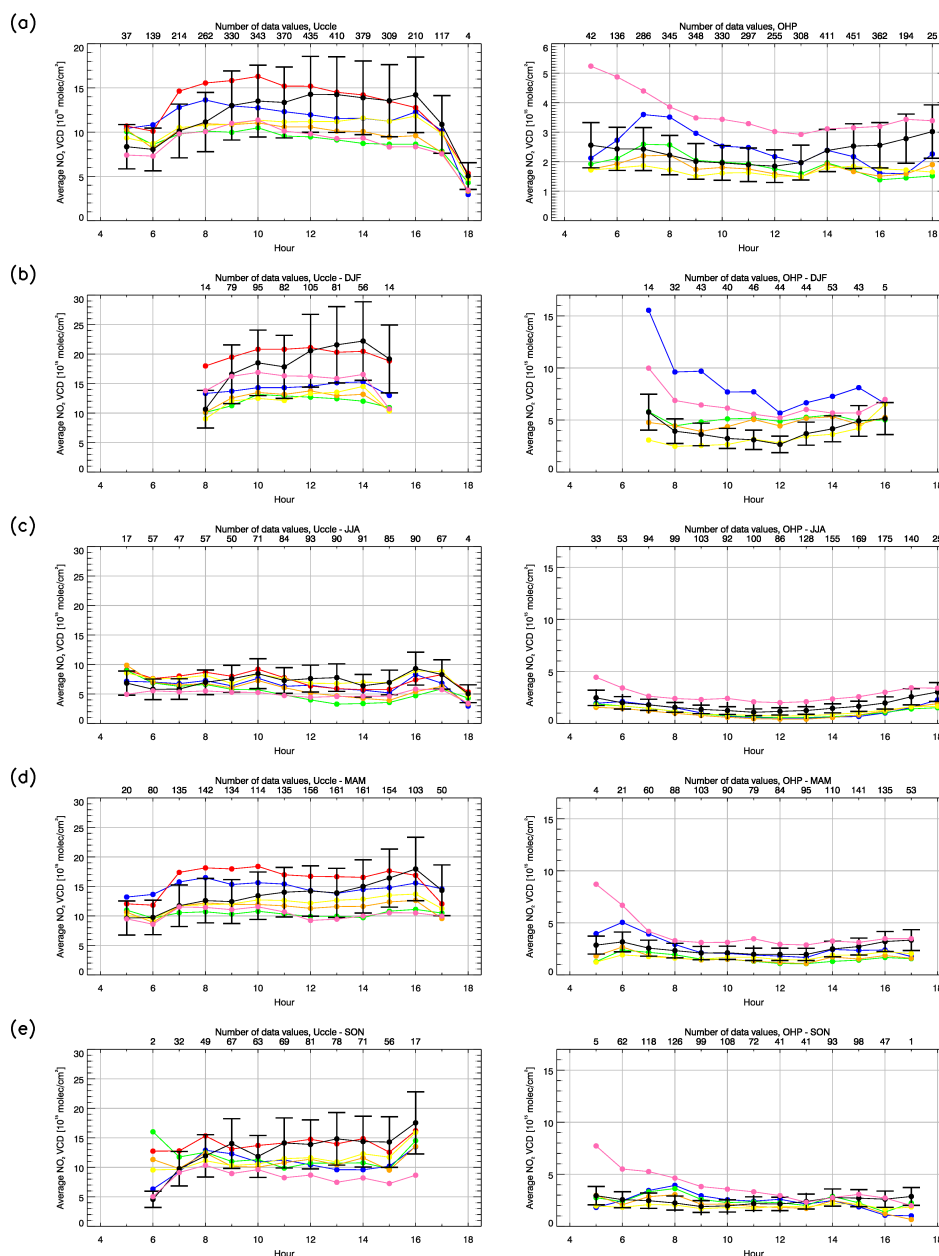
Figure A13. As in Figure 9 but for separate model runs: (blue) LOTOS-EUROS, (yellow) CHIMERE, (green) EMEP, (orange) EMEP-MACCEVA, (pink) SILAM and (red) MOCAGE.

Atmospheric
Chemistry
and Physics
Discussions

Open Access

EGU
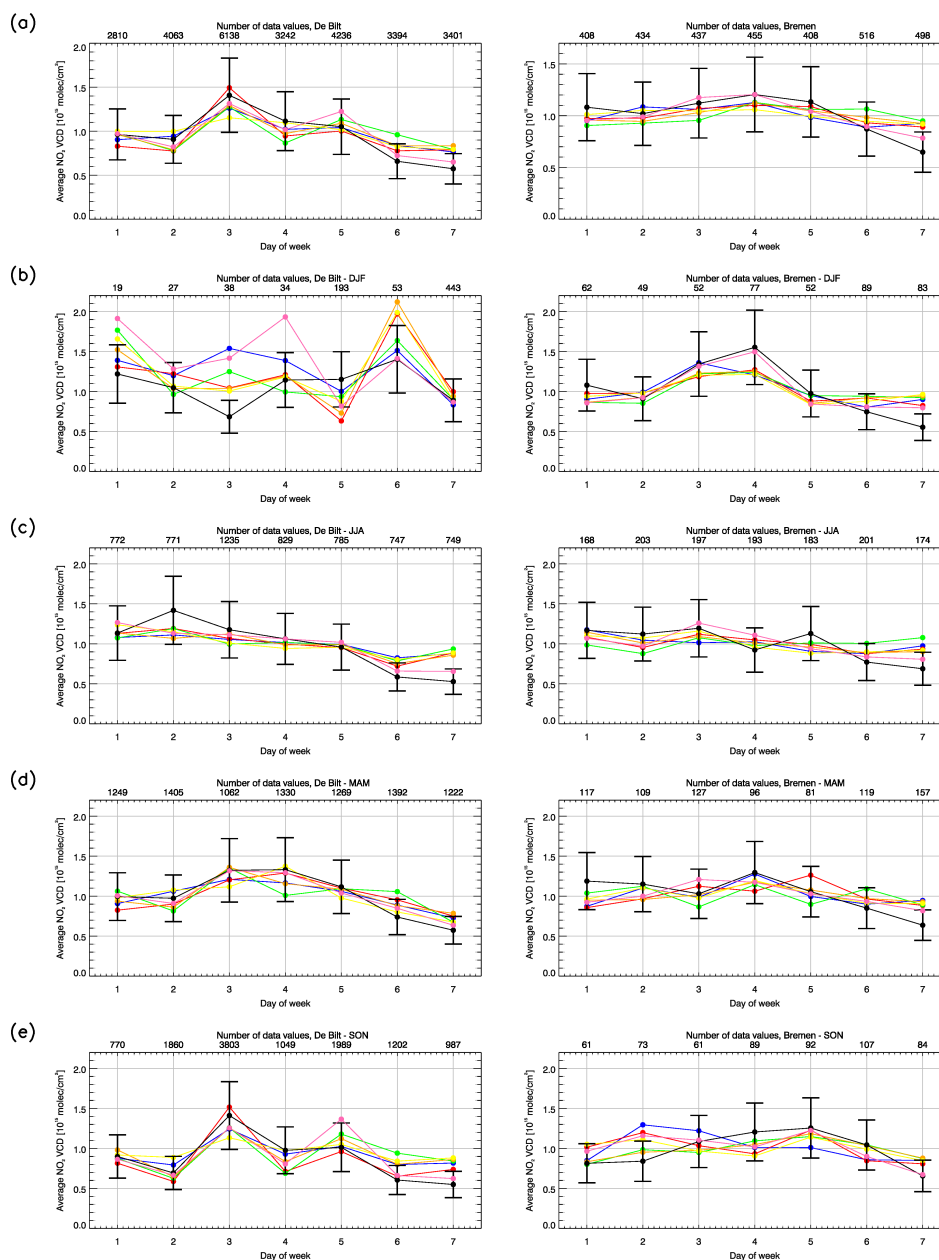
Figure A14. As in Figure 10 but for separate model runs: (blue) LOTOS-EUROS, (yellow) CHIMERE, (green) EMEP, (orange) EMEP-MACCEVA, (pink) SILAM and (red) MOCAGE.

Atmospheric
Chemistry
and Physics
Discussions
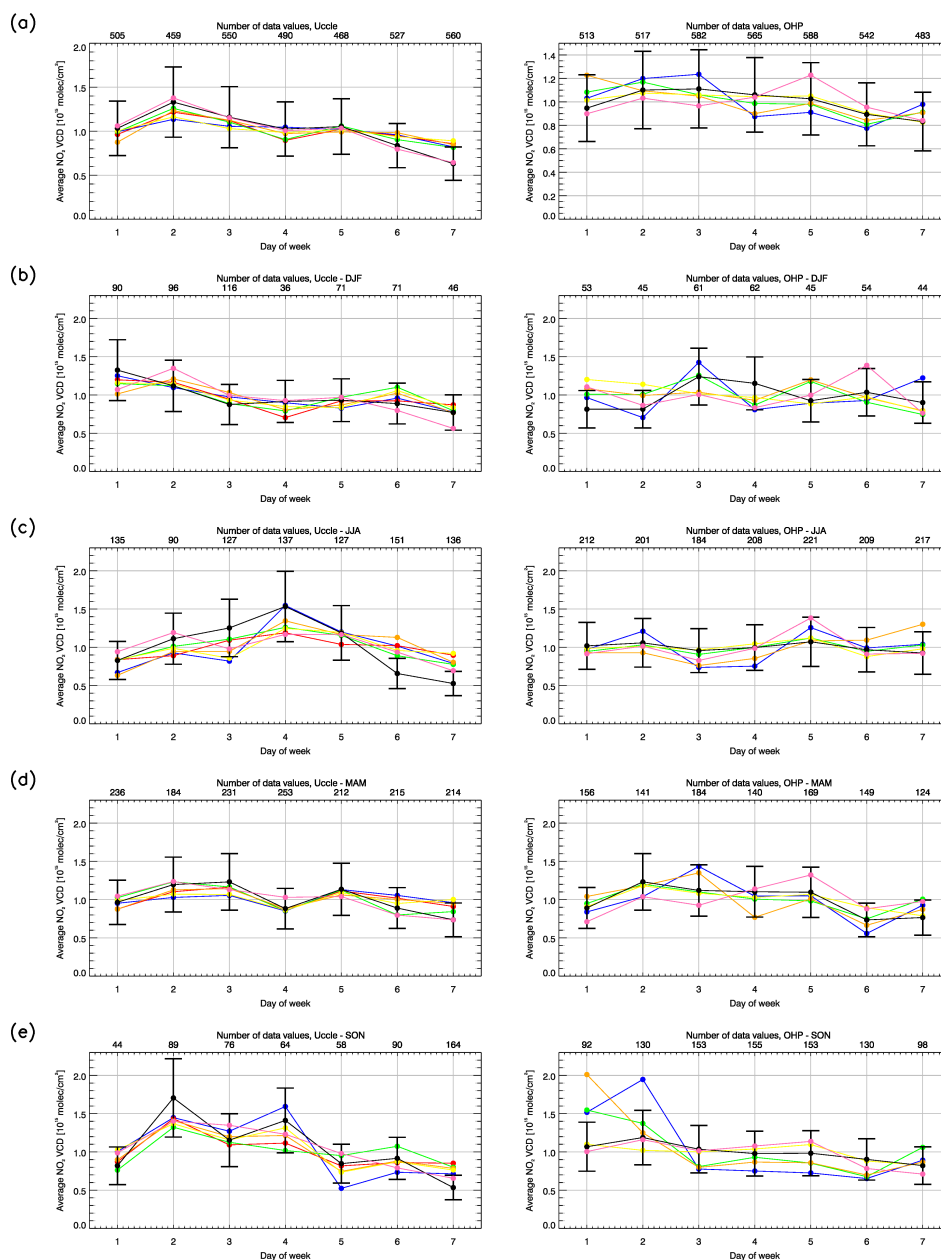
Figure A15. As in Figure 11 but for separate model runs: (blue) LOTOS-EUROS, (yellow) CHIMERE, (green) EMEP, (orange) EMEP-MACCEVA, (pink) SILAM and (red) MOCAGE.